NBSIR 78-1523

Numerical Solution of the Electron Slowing-Down Equation for Molecular Hydrogen

L. V. Spencer

Center for Radiation Research
National Measurement Laboratory
National Bureau of Standards
Washington, D.C. 20234

and

R. Pal

Howard University
Washington, D.C. 20059

December 1978

U.S. DEPARTMENT OF COMMERCE
NATIONAL BUREAU OF STANDARDS

NBSIR 78-1523

NUMERICAL SOLUTION OF THE ELECTRON SLOWING-DOWN EQUATION FOR MOLECULAR HYDROGEN

L. V. Spencer

Center for Radiation Research
National Measurement Laboratory
National Bureau of Standards
Washington, D.C. 20234

and

R. Pal

Howard University
Washington, D.C. 20059

December 1978

U.S. DEPARTMENT OF COMMERCE, Juanita M. Kreps, *Secretary*

Dr. Sidney Harman, *Under Secretary*
Jordan J. Baruch, *Assistant Secretary for Science and Technology*
NATIONAL BUREAU OF STANDARDS, Ernest Ambler, *Director*

NUMERICAL SOLUTION OF THE ELECTRON SLOWING-DOWN EQUATION FOR MOLECULAR HYDROGEN

L. V. Spencer
National Bureau of Standards
Washington, D.C. 20234

and

R. Pal
Howard University
Washington, D. C. 20059

ABSTRACT

Procedures are outlined for solution of the slowing-down equation for fast electrons by direct numerical integration. Spectra for H_2 are computed by use of Gerhart's cross section set, suitably modified, and with inclusion of vibrational excitations. The flexibility and stability of the approach is demonstrated by solutions for source energies ranging from 1 MeV down to 24 eV with the spectrum extended below 2 eV. Energy and number conservation are checked in detail, and the ionization yield is computed as a function of energy. Spectrum and ionization yield so obtained are compared with previous calculations; general agreement is found with some significant differences. Agreement with Combecher's measured ionization yields at low energies is rather satisfactory overall, but with significant deviations of trend. Some exploration of secondary and tertiary electron contributions is included.

Key words: Electron slowing-down; energy degradation spectrum; inelastic cross section set; ionization yield; molecular hydrogen; W-value.

NUMERICAL SOLUTION OF THE ELECTRON SLOWING-DOWN EQUATION FOR MOLECULAR HYDROGEN*

L. V. Spencer and R. Pal

I. Introduction

Electron energy degradation or "slowing-down" is due to inelastic interactions with the surrounding medium. The process generates a spectrum $\underline{y}$ which expresses the relative likelihood that a fast electron is detected in different energy intervals dT. More specifically, ydT can be considered as the expected value of the pathlength traveled by a source electron, together with that by secondary electrons which it generates during the slowing down process, while the one or any of the others have kinetic energy within dT.

The importance of y derives largely from the fact that one need only multiply $\underline{y}$ by the (suitably normalized) cross section for some process, and integrate over all electron kinetic energies, to obtain the yield for that process, whether excitation or ionization. But given a correct spectrum $\underline{y}$, the resulting yields are no more accurate than the cross sections which are used to evaluate such integrals. Errors in evaluation of the slowing-down can accentuate and greatly complicate the errors and uncertainty of any yields so calculated.

There are two difficulties associated with determining the energy degradation spectrum. First, the inelastic scattering cross sections are complex and hard to obtain. Secondly, because of the complexity of the cross sections the numerical solution of the transport equation is not a trivial task. As a result there have been nemerous investigations with various types of approximations which will be briefly reviewed below. But since the basic integral equation of which $\underline{y}$ is the solution can in principle be solved by standard numerical techniques, we feel that it is appropriate to make an

---

*Supported in part by the Office of Naval Research.

attempt to do this. This paper describes a successful calculation of $\underline{y}$ for molecular hydrogen by application of well-known numerical integration techniques to the standard form of the slowing-down equation. Because the cross sections utilized are current the resulting data is of general interest.

Before proceeding to describe this effort, we identify some of the other methods which have been applied in the following section, two of the most recent (for H_2) being due to Douthat [1] and to Garvey, Porter, and Green [2]. Our comparisons with results from these and other calculations are of interest perhaps more because different cross section sets have been applied than because of contrasting computational methods. We use the cross section compilation of D. E. Gerhart [3]; but we must modify Gerhart's forms to render them more readily applicable to our procedures, as well as to make extensions to relativistic energies. In addition, we take account of vibrational modes in order to extend our results well below the threshold for electronic excitations, i.e. down to about 1.5 eV.

We believe that the calculations described here are significantly more accurate than previous evaluations of $\underline{y}$ for molecular hydrogen. Comparison with recent measurements of the ionization yield as a function of electron source energy can be construed as pointing out the importance of more accurate ionization and excitation cross sections in the range from 15 eV to perhaps 30 eV for future improvement of both slowing-down spectrum and yield results.

New aspects explored here include careful and complete checks of energy conservation and conservation of the number of primary particles. In addition, the spectral structure near the source energy is resolved in its most important features; and there is some discussion of general characteristics of spectral structure, particularly as it results from those generations of secondary electrons which are its most important components.

II. Comments on Computational Methods

If electrons are generated with initial kinetic energy T_0, the slowing-down equation of which y is the solution is

$$K(T)\, y(T,T_0) = \int_T^{T_0} dT'\, k(T',T)\, y(T',T_0) + \delta(T-T_0) \quad , \qquad (1)$$

where $K(T)$ is the total inelastic interaction probability per unit pathlength at kinetic energy T; and $k(T',T)dT$ is the differential probability, per unit path length, for an electron of energy T' to undergo an interaction resulting in an electron having kinetic energy in the interval dT containing T. This electron can be a new secondary, or the result of an energy loss $(T'-T)$. The Dirac delta function in eq (1) describes a monoenergetic source of unit strength with kinetic energy T_0; and the spectral function $y(T,T_0)$ has dimensions path length per unit energy.

Direct numerical integration of eq (1) has not been thought very feasible because of the general structure of $k(T',T)$ for T' near T. A large and complex concentration of interaction probabilities occupies a narrow region 11 eV $\lesssim T'-T \lesssim$ 18 eV, as seen in Fig. 1. Further, for whatever value of T_0 may be selected, energies within a few tens of eV of T_0 can only be reached if no more than one, two, or at most a few interactions have occurred. This means that the structure for T' near T in the cross sections also appears for T near T_0 in $y(T,T_0)$. Thus the integrand of eq (1) has complicated features for T' near T, and for T' near T_0; and these two regions of structure both make significant contributions to the integral. Direct numerical integration must therefore deal with the necessity to use integration steps perhaps less than 1 eV wide to resolve structure, while at the same time covering an energy range below T_0 that can be of the order of 10^6 eV or greater.

Most calculations with T_0 above a few hundred eV have attempted to bypass the complexities of $y(T,T_0)$ for T near T_0. Incidentally, this structure was first described by H. W. Lewis, and therefore has been called the "Lewis effect" [4]. The various computational methods fall into distinct classes as follows:

(1) Numerical evaluation of an integral form of eq (1). If one integrates all terms of eq (1) over the variable T, from a value $\bar{T}$ (say) to the source energy T_0, one obtains an equation of balance for the number of electrons with kinetic energy above $\bar{T}$.[1] A similar integral over all terms in which an additional weighting factor T is used in the resulting integrands, gives a corresponding equation of balance or "conservation" for energy flowing into, and out of, the reservoir of electrons with kinetic energies between $\bar{T}$ and T_0.[1] These conservation equations exhibit the significant advantage of having kernel functions with less irregular and singular trends than eq (1). Further, conservation of number or energy is usually more important than a detailed description of cross section structure, when one attempts to solve for y at most spectral energies. A number of authors have successfully used the "number balance" equation (eq (7)) to obtain solutions for y [1,5-10].

(2) A more elementary and older method, which is sometimes used to obtain approximate solutions to the slowing down equation employs the continuous slowing down approximation (CSDA) [11-15]. While the CSDA is more suited to the slowing down of heavy charged particles, it also describes in a rough way the consequence of the frequent, small-loss interactions of electrons with the medium through which the electrons move. One can readily derive this

---

[1] See eqs (7) and (8).

approximation from eq (1). Any electron, once generated, contributes a term $1/S(T)$ to the slowing-down spectrum below the energy at which generated, where $S(T)$ is the stopping power; and the number of secondary electrons generated can be calculated from a much simplified integral equation. Calculations of this type give a good general description of $y(T,T_0)$ which can be sufficiently accurate for some purposes. They are easily developed and inexpensive, but they are not highly accurate.

(3) Monte Carlo methods can be used to evaluate the slowing-down spectrum as an average over a few, or perhaps a few hundred or thousand case histories [16-19]. All that is required for good statistics is many collisions in each energy interval specified. Since each source electron not only remains a part of the calculation to very low energies, but also gives rise to many secondaries, the statistics actually improve as the calculation progresses to low energies. Energy conservation can be readily imposed by insuring that all energy resulting from each interaction is properly accounted for. The Lewis effect region can be described if and as desired. Hence results obtained by use of this method can be impressive. Perhaps its main drawback is the time required to calculate each case history, which makes computations of many case histories with high source energies comparatively expensive.

(4) Use of a discrete analog, in which electrons progress from higher to lower energy "bins" according to computed transition probabilities between pairs of bins. Mostly, such calculations have been used with rather low source energies (e.g., $\lesssim$ 1 keV) [20-24]. A recent publication gives results of systematic calculations of this type to much higher energies [2]. The authors of this last paper chose an interval near the source energy sufficiently wide that the Lewis effect was wiped out; but they indicate that the method can be extended to give a more detailed description if desired.

(5) Use of methods which solve an equation adjoint to eq (1) [3,24-28]. Such equations have a form similar to eq (1); but the solution progresses upward in energy rather than downward. Difficulties with the integration process are not removed, because the complexities of the function $k(T',T)$ remain. These calculations usually evaluate yields directly, rather than $y(T,T_o)$. Most such calculations have been performed at low energies (up to 1 keV); and the development of a wide variety of methods to solve these equations is still in process.

(6) The application of numerical integration to eq (1), which is the subject of this paper, and which has greatest resemblance to method (4), that is, use of a discrete analog. Here one attempts to apply standard techniques of numerical integration to the evaluation of the scattering integral, for T values which progress stepwise to lower energies. some use of this method at low energies is reported by Douthat [1].

We know of two attempts to make comparisons of the different methods when the same, or closely similar, cross sections are being used [23,24]. The more recent study features W, the reciprocal of the ionization yield, as an integral comparison parameter [24]. It gives little information on relative accuracies of different types of computations of $y(T)$. The earlier study [23] compared CSDA results for He and N_2 with results obtained by the discrete analog method. Only electron sources of 500 eV and below were used. Differences are significant; but qualitative and rough quantitative agreement are found. One reason for attempting to apply direct numerical integration systematically is the possibility that accuracy for a given cross section set can thereby approach ~ 1%. This would effectively eliminate computational methods as a source of significant error in evaluation of slowing-down spectra or yields. Such accuracies probably require a more detailed evaluation of the Lewis effect region; but this can be desirable on its own merits.

A certain amount of structure occurs at low energies in the slowing-down spectrum also, because the thresholds for different types of transition can give rise to irregularities. We think that this structure can be more easily evaluated by direct integration of eq (1) than by use, e.g., of integral forms of the transport equation (method (1) preceding).

Successful methods for direct numerical integration also can in principle be used to evaluate space and directional aspects of electron transport by methods not heretofore applied with realistic cross section data to this type of particle transport.

Because the systematics of slowing-down spectra are important for obtaining similar spectral information about materials and source energies not otherwise studied in the same detail, we have organized the calculations to permit identification of the primary electrons as well as the 1st, 2nd, and higher generations of secondary electrons. The different generations play rather different roles; and their spectral components require a somewhat different description for each generation.

One problem avoided in our calculations for H_2 is the problem of inner shells. While hydrogen has only one shell, most other materials of interest have inner shells. In the kernel function $k(T',T)$ different atomic or molecular shells can contribute terms describing electrons with the same kinetic energy T; so one must in principle include calculations for all contributing shells whenever k is required. These calculations must be performed many times, because k appears as a factor at each step of each integration. We do not see any fundamental difficulty in this requirement, although it surely increases the computational time of calculations by any method.

A related problem which likewise appears only in materials with $Z > 2$ is that of including Auger electron components. These have energies characteristic of transitions between different shells. They must be treated as an additional source whose inclusion is necessary for conservation of energy. Again, there appears to be no fundamental difficulty in accounting for this component; but our current task is simplified by their absence from H_2 spectra.

III. Cross Sections and Stopping Powers

The shape of the differential cross sections has a dominant influence on integration procedures appropriate for this and other similar problems. Section IV, which follows, illustrates this in detail. In this section we give general information about the set of differential cross sections with which we work, and the total cross section and stopping power data derived from it. More details about these cross sections are given in Appendix I.

We have adopted a well-known set of cross sections for our calculations, namely the H_2 cross section set developed by Donald E. Gerhart in his PhD thesis [3]. Gerhart followed Platzman's use of the Weiszäcker-Williams approach in which collisions are classified as either hard or soft, but not both. This involves specifying cut-offs to both soft ("glancing") and hard ("knock-on") collisions.

In the process of adapting these cross sections to our use, we have made a number of modifications. A brief summary of these changes is as follows: 1) We have extended Gerhart's cross sections into the relativistic range in a manner which gives stopping powers of the Bethe theory type, with reasonable

values for the "mean excitation potential", here designated ⟨I⟩. 2) In addition, we have modified the form of Gerhart's cut-off function for small energy losses due to hard collisions; for our purpose it is more advantageous to use an abrupt, rather than gradual cut-off of this kind. 3) At low electron kinetic energies, where the differential spectrum of energy losses is poorly known,extend the use high energy cross section forms by ad hoc adjustments of the cut-off for momentum transfers, which is a constant at high energies in cross section formulae for glancing collisions. This replaces an abrupt transition at 350 eV to low energy forms which Gerhart used, while preserving good agreement with total ionization cross sections. 4) We have added vibrational excitation cross sections which were omitted by Gerhart, and which play a dominant role for kinetic energies below about 12 eV. 5) Finally, we symmetrized the glancing collision cross sections. These matters are given in greater detail in Appendix I, which also contains additional numerical information omitted from Gerhart's publication, such as a set of transition energies for the discrete part of the spectrum as given by Namioka [29].

In the process of satisfying sum rules, Gerhart adopted an oscillator strength distribution (OSD) which gives a value for the ionization dipole strength ~ 10% lower than data from other sources, with OSD values for the excitation region correspondingly a little higher than other data. We doubt that this is desirable, and one of us (RP) has developed an OSD safisfying the sum rules without such adjustments. But the importance of Gerhart's cross sections is such that we have used them -- with modifications as outlined above -- in the extensive numerical explorations reported here.

Figures 1 and 2 present differential cross section data as calculated by our version of Gerhart's cross sections. Figure 1 displays the variation with energy loss. Figure 2 shows that our version of Gerhart's cross sections agrees rather well in shape with the Opal, Beaty, and Peterson [30] experimental data for the spectrum of secondary electrons at $T = 500$ eV. One should note, however, that the experimental data have been divided by a scale factor of 1.65.[2] A similar comparison at $T = 100$ eV with recent experimental data due to Rudd and Dubois [31] shows somewhat poorer agreement as to shape, but better agreement in magnitude. In both cases, the experimental data appear to drop below the theoretical data at very low secondary electron energies.

Figures 3 and 4 present stopping power and total cross section results. Values for the stopping power obtained using Bethe's expression are also given in fig. 3, as are some recent unpublished data due to Green [32]. Gerhart's OSD leads to a computed value for $\langle I \rangle$ of about 19.2 eV as stated in his paper [3]; and this value was used in calculating the curve labeled "Bethe". On the other hand, our set of cross sections leads to an equivalent constant with the value $\langle I \rangle_p = 18.6$ eV even though utilizing Gerhart's OSD. While it is possible to make adjustments which would increase the latter value, we have not attempted to do so. See Table I.6 for other data on $\langle I \rangle$, both experimental and theoretical.

---

[2]This means that the Opal, Beaty, Peterson data extrapolated in a reasonable way give an integrated value significantly larger than data due to Rapp and Englander-Golden [33], to which Gerhart's cross sections are normalized.

IV. General Method of Solution

A. Comments on the integration

In solving integral equations such as eq (1), the usual approach involves replacement of the integral by a weighted sum as follows:

$$\int_{T_n}^{T_o} dT'\ k(T',T_n)\ y(T',T_o) \approx \sum_{i=1}^{n} w_i\ k(T_i,T_n)\ y(T_i,T_o) \quad . \qquad (2)$$

If all values $y(T_i,T_o)$ are known except for $y(T_n,T_o)$, and if all values for w_i have been specified, eq (1) gives a value for $y(T_n,T_o)$.

When both factors of the integrand vary smoothly and slowly from one value of T_i to its neighboring values, weights w_i can be adopted from one of the standard formulae, such as Simpson's rule or even the trapezoidal rule. This method of calculation is suitable for regions in which $k(T',T)$ and $y(T,T_o)$ vary with similar rapidity and irregularity, because the many values for T required to describe such functions correspond rather well in spacing and number to the mesh of values required to evaluate the scattering integral accurately.

An altogether different circumstance can occur, however. One of the factors in the integrand can be rapidly varying while the other is smooth, slowly varying, and predictable. Thus for large T_o, at most kinetic energies T', $T' < T_o$, one has a slow and predictable function $y(T',T_o)$ combined with very rapid and irregular variations of $k(T',T_n)$ whenever T' is within perhaps 30 eV of T_n. This is well-illustrated in fig. 1, where the cross section, which is proportional to k, is given as a function of the difference

between the variables. The irregular behavior for $(T_o - T)$ or $(T' - T_n)$ between 11 eV and 25 eV occurs for virtually all T_n, regardless of trends of y.

Under these circumstances eq (2) is still appropriate; but it is no longer desirable to use elementary numerical integration weights. Instead, one can use integrals over k, usually moments, to construct an approximation to k as a sum of Dirac delta functions. The integral is then readily performed and gives an expression of the type shown by eq (2). We refer here to such "δ - function approximations" by the general designation "Gauss quadrature" (GQ).[3]

The simple numerical integration algorithms for the solution of eq (1) on the basis of expressions of the type illustrated by eq (2) require the T_i to have the same values for different T_n. Other algorithms are possible; but this is preferable on the basis of simplicity. We thus choose T_i values for the complete calculation at the start, with T_n's which march down this preselected list. To achieve accuracy comparable with Simpson's rule in eq (2), we evaluate three energy moments of k for the combined pair of intervals $T_{n-2} \leq T' \leq T_n$. The resulting three conditions[3] fix δ-function weights at T_n, T_{n-1}, T_{n-2}. These weights can be cumulated with other weights, since all play the same role in the numerical integration at various T_i values of the same set.

---

[3]We here include the option of pre-specifying some or all x_i values. This results in a unified view of numerical integration procedures of many types. The usual Gauss quadrature can be considered as an approximation of the type $w(x) \approx \sum_{i=1}^{N} \alpha_i \delta(x-x_i)$, where the α_i and x_i are fixed by $2N$ moment integrals. In the classic case, the weight function $w(x)$ is unity for $-1 \leq x \leq 1$. For another well-known case $w(x) = e^{-x}$, with $0 \leq x \leq \infty$.

By restricting our approach to integration formulae which yield sums of the type shown in eq (2), we can determine w_i values by two or more different procedures of this type, each appropriate to a sub-region of the domain of integration.

B. The integration mesh

Description of the Lewis effect, i.e. resolution of complex spectral details near the source energy, requires that intervals for numerical integration be ≤ 1 eV, as already noted (see fig. 1). Similarly, at low energies, near and below the ionization potential, trends of $y(T,T_o)$ with T are again steep, with possible structure. Small intervals are therefore also appropriate for solution of the integral equation at low energies. But it is quite clear that most of the energy range, that between, say, 100 eV and $(T_o - 100)$ eV, does not require such a detailed description because $y(T,T_o)$ has trends which are smooth and not particularly rapidly varying.

Our choice of the energies T_n constituting the solution mesh was therefore as follows: We used the tabulation intervals established for the OSD to develop a set of T_n values in the energy range from T_o down a total of 40 to 80 eV lower in energy. The interval size was then increased abruptly from $\Delta T \sim 2$ eV to $\Delta T = 20$ eV. Following this, the intervals were increased in geometric progression until the energy loss amounted to $T_o/2$. Typically, then, the energies T_n, such that $T_n < T_o/2$, were equated to the energy losses $(T_o - T_n)$. Thus the solution energies were approximately twice in number those required to carry the solution from T_o to $T_o/2$.

The reason for an abrupt change in interval size as referred to above is that intervals smaller than 2 eV can resolve at least moderately well the main features of the glancing collision region, even between 13 and 17 eV. On the other hand, intervals greater than 20 eV are large enough so that the

whole band of irregularities in $k(T',T)$ is contained within a single interval; and fine resolution is then rendered unnecessary except in regards to the calculation of GQ weights, which is accomplished by interpolation on basic tables of cumulative integrals.

We did find it convenient to buffer the transition to large intervals with two intervals of size 10 eV, at the same time ensuring that the GQ region extended beyond one such interval. Table 1 gives an illustrative set of T_n values, for a 1 keV source.

From the attention given to such details, it should be evident that setting up a suitable integration mesh constitutes a significant part of our calculation. Typically, the fine spacing for high and low energy regions requires about 40-45 points each, with up to 90 additional points assigned to the remaining (usually large) energy region. We used up to ~ 200 integration points, so that instruction and data memory components together occupied just under 64 K cells of the memory.

C. The integration procedure

Both glancing and knock-on cross section components have a rather simple analytic structure; thus $k(T',T)$, with $T' = T + E$, has the form

$$k(T+E,T) = \sum_i f_i(T+E)\, g_i(T,E) \quad . \tag{3}$$

The functions $f_i(T + E)$ are slowly varying, and the functions $g_i(T,E)$ can either be integrated analytically, or depend only on E, or both. We have already mentioned tabulations of cumulative integrals of the (rapidly varying) $g_i(E)$ for glancing collisions. Corresponding functions $g_i(T,E)$ for knock-on collisions can be integrated analytically.

Because the functions $f_i(T + E)$ are slowly varying, if combined with the function $y(T + E, T_o)$ the product tends to vary slowly or rapidly according to the characteristics of y. This leads us to pretabulate the f_i at the solution energies T_n, with integration based on variables G_i defined by

$$\frac{dG_i}{dE} = g_i(T,E) \quad . \tag{4}$$

Then

$$\int_T^{T_o} k(T',T)\, y(T',T_o)\, dT' = \sum_i \int dG_i\, f_i(T,G_i)\, y(T,G_i,T_o) \quad . \tag{4'}$$

This approach should be contrasted with the more direct procedure of simply evaluating $k(T',T)$ as necessary for all combinations (T_j,T_n) which appear in the set of integrations. We have ordinarily used 5 or 6 terms, i.e. values of i, so that the right side of eq (4') has ~ 6 terms in the sum. On the other hand, pre-tabulation of the f_i is quick and cheap, because it need be done only once to obtain a list of values for all solution energies T_j. By contrast, direct evaluation of $k(T',T)$ requires calculations of all component factors of k for a quadratic, rather than linear array, more or less cancelling out any extra computer time required by the multiplicity of i values. In addition, by differencing G_i we readily obtain the lowest moment required for the GQ; repetitious tabulations to evaluate GQ moments are avoided by use of several such cumulative functions.

We believe that it would be about equally feasible to use tabulations of cumulative G_i integrals for the Gauss quadrature, with direct evaluation of $k(T',T)$ reserved for evaluation of the remainder of the scattering integral; but we have thus far chosen not to proceed in this way.

We always use GQ for the final interval, $T_{n-1} > T' > T_n$, and we use a version of Simpson's rule for the remainder of the scattering integral. Our GQ contribution to eq (2) is as follows:[4]

$$\int_{T_n}^{T_j} dT'\ k(T',T_n)\ y(T',T_o) \approx W_1 y(T_{j+1},T_o) + W_2 y(T_j,T_o) + W_3 y(T_{j-1},T_o), \quad (5)$$

where j is commonly, but not always, equal to n-1. Since $k(T',T)$ vanishes for $(T' - T) < 11.2$ eV, we find it advantageous to extend the GQ interval to fully cover this gap, because other integration procedures are rendered inaccurate when extended into a region in which the integrand is zero. The rule adopted for choice of j is therefore that it equal the largest m value such that $(T_m - T_n) > 11.2$ eV.

Six cumulative integrals over the OSD giving data for three energy moments (see Appendix I), together with corresponding analytic integrals over components of the knock-on cross section, give moments of the different $g_i(T,E)$ from which integration weights can be systematically developed for all j values by combining contributions from adjacent integration intervals, each covering two intervals of the tabulation.

---

[4]Note that T_{j-1} need not be included between T_n and T_j.

We should comment that in integrals of the type shown on the right of eq (4'), for all ranges except those where GQ is applied we systematically use

$$dG_i = \frac{dG_i}{du}\, du \quad , \tag{6}$$

where for each three consecutive T_i values the corresponding u values are -1, 0, and 1, thus permitting application of the elementary form of Simpson's rule. We determine dG_i/du by fitting each three consecutive G_i values to a quadratic in u. Note that only two of the six cumulative integrals over the g_i are required for this process; we use the other information available in Table I.2 only for the GQ.

D. Energy and number conservation

In order to monitor the calculations very closely we wrote a special subroutine (ECHEK) to perform energy conservation checks at selected energies $\overline{T}_n$ (see Appendix II). The integral forms of the slowing-down equation which were referred to in the introductory discussion are (for energy conservation)

$$\int_{\overline{T}}^{T_0} dT'\, S(T',\overline{T})\, y(T',T_0) = T_0 \quad , \tag{7}$$

where $S(T',\overline{T})$ is a limited stopping power which excludes energy transfers to secondary electrons with kinetic energies exceeding $\overline{T}$. For number conservation the equation

$$\int_{\overline{T}}^{2\overline{T}+I} dT'\, K_p(T',\overline{T})\, y(T',T_0) = 1 + \int_{2\overline{T}+I}^{T_0} dT'\, K_s(T',\overline{T})\, y(T',T_0) \tag{8}$$

holds, where $K_p(T',\overline{T})$ and $K_s(T',\overline{T})$ are, respectively, the probabilities per unit path length for removal and addition of an electron to the kinetic energy interval between $\overline{T}$ and T' [5]. Accurate evaluation of the integrals in eqs (7) and (8) is of comparable difficulty to the main problem of evaluating eq (1), although one can use devices that have previously proven satisfactory [5-10]. The accuracy of the numerical integration remains a problem because $S(T',\overline{T})$ and $K_p(T',\overline{T})$ give important contributions for $(T' - \overline{T})$ small, while retaining some irregularity.

For evaluation of eqs (7) and (8) we wrote a general stopping power subroutine (STN) and an integrated cross section subroutine (TCX) according to a pattern which permitted rapid and simple cumulative integration over transition energies up to an arbitrary limit (see Appendix II). These routines were essential to the evaluation of the kernel functions of eqs (7) and (8). In preparing the stopping power subroutine, all contributions due to the energy of ionization must be sometimes, though not always, included. This requires a special term when fast (i.e. above cut-off) secondary electrons were generated.

In the use of both stopping power and integrated cross section subroutines, one must bear in mind that for $T' < 2\overline{T}_n + I$ both primary and secondary electrons from an interaction can lie below the energy cut-off $\overline{T}_n$. For such interactions the total energy of the electron being scattered is "dissipated."

The exercise of taking account of energy conservation has proved necessary and very instructive. By this means we found that in the transition from finely spaced integration intervals to coarse integration intervals, some of the energy (typically $\sim 4\%$) can be lost. This may be partly due to the fact that the changeover necessarily occurs sufficiently near the source energy to

be affected by the Lewis effect irregularities. The first few points with coarse spacing are uncertain by a few percent for this reason; and any resulting error is then "locked" in, because the major contribution to the scattering integral is always due to a few points thus affected.

To correct such errors, we have calculated energy conservation as well as a value for y_i at the first five T_i values with the coarse spacing. We adjusted these y_i values immediately as if any deficiency of energy conservation were solely due to the y_i value being determined. This worked well.

In general, we find that energy-conservation results give a good check on the accuracy of the computations. The number conservation data are in numerical agreement with energy conservation data above $T_o/2$. Below $T_o/2$ the number conservation data simply record the total number of fast electrons generated by all processes. But the number conservation check can be extended to very low energies by applying it to the primary electron component only.

E. Special features

At the time the computer program was being written, we felt that it might be very important to distinguish between primary electrons, the first generation of secondary electrons, and higher generations of secondaries. Hence in setting up the basic table of integration weights, we arranged for two types -- i) those including, and ii) those not including the secondary electron components of the scattering integral. The former are used to compute the full slowing-down spectrum; the latter, together with the difference between the two types, are necessary for computation of the different generations of secondaries. To economize memory storage space, these two triangular arrays of integration weights are both stored in the same nearly square array (called WT).

Table II.1 gives a summary description of the computer program which we developed, and which we call ELSPEL, for Energy Loss Spectrum of Electrons. Discussion of each of the eighteen routines is presented in Appendix II.

IV. Discussion of Results

A. Energy Conservation

We begin our discussion of results with a table showing typical energy and number conservation data, i.e., table 2. A value of unity is the desired result, and departures from unity indicate fractional differences from source energies T_0. Such departures are seen to approach a few percent, although for most energies the agreement is $\sim$ 1%. Since the integrals required for these checks feature a large contribution from the region of T' near T, the departures from unity of table 1 are partly due to evaluation of the energy conservation integral, in addition to errors of y. But for the most part, we believe that the energy conservation integral is a reliable measure. The results shown are sufficient to demonstrate a general feasibility of the approach which we have developed. Further improvements in computational accuracy can no doubt improve this check. One should note that the rate of change of the energy conservation data is probably a better indication of the accuracy of y in any given part of the spectrum than are the values shown.

Figure 5 gives the fractional contribution to the energy deposition by primaries, secondaries, and all other components combined. Here, energy deposition includes energy losses of all types except the kinetic energies of secondary electrons still capable of ionizing, i.e. kinetic energies > 16 eV. There is evident a rather remarkable persistence of the importance of the primaries and first generation secondaries, which together are responsible for more than 90% up to source energies greater than 300 keV. Since both

components can be represented rather well with fairly simple functional forms, one can hope to obtain analytic representations in this manner which are usable for many types of yield calculations.

B. The Lewis effect

Figure 6 demonstrates the Lewis effect and its main features at a single (high) source energy (1 MeV). The abscissa measures the energy loss in eV. The Lyman and Werner bands appear as peaks, with multiple interactions producing a similar structure which decreases in prominance. The maintenance of the similarity of structure for multiple interactions is very likely due to the dominance of the Lyman peak: probably all but one of the interactions combining to give prominent secondary and tertiary peaks are Lyman interactions.

While not evident, the peaks of fig. 6 are in reality composed of many individual lines which are not resolved. It is possible to resolve these lines with finer spacing, but we have not seen fit to attempt it.

The rather arbitrary cut-off of low-energy knock-on interactions leads to a rather small discontinuity, labled "Møller," which is identified on the figure. The form chosen for this cut-off is evidently not very important. Also displayed is the energy-loss region for which energy conservation is used to correct the solution. The smoothness apparent in this region is partly an artifact of the method used, and partly a consequence of increased interval size, both of which act to wash out the physical irregularities.

The ordinate has been chosen so that at large energy losses the curve in fig. 6 should approach unity, corresponding to the increasing validity of the reciprocal stopping power approximation for $y(T,T_o)$. This result is apparent although the asymptotic trend develops more slowly at larger source energies than we would have expected.

C. Properties of slowing-down spectra

Figure 7 presents spectra for four source energies. The ordinate has been chosen so that the curve is fairly flat in the region of dominance by secondary electrons.[5] For the 30 keV case, contributions by primaries and first-generation secondaries are indicated by dashed lines; and in the case of the primaries, the dashed line has approximately the functional form T/T_o.

According to the CSDA approximation, the first generation secondary electrons due to a monoenergetic source at T_o are described by

$$y^{(1)}S = \int_{2T}^{T_o} dT' \; K_s(T',T)/S \quad , \tag{9}$$

where K_s is the kernel function of eq (8). If we write the stopping power in the form $S = \kappa(T)\, B(T)$, where $B(T)$ is the stopping number, then the lead term of K_s/S is $[T^{-1} + (T' - T)^{-1}]/B(T')$. We assume $T_o >> T$ and make use of the usual slow rate of variation of $B(T')$ in evaluating this factor at $T' = T_o/2$, which is approximately the midpoint $(T_o + 2T)/2$ of the integration interval. Then,

$$\frac{T}{T_o}\, S(T)\, y^{(1)}(T,T_o) \approx \frac{1}{B(T_o/2)} \left[1 - 2\frac{T}{T_o} + \frac{T}{T_o} \log \frac{T_o - T}{T}\right], \; T < T_o/2$$

$$\approx 1/B(T_o/2), \; T << T_o. \tag{9'}$$

The minima of the weighted spectra shown in fig. 7 are thus expected to have roughly the value $1/B(T_o/2)$, due to 1st-generation secondaries which

[5] Since the product $S \cdot y$ is a rough measure of the number of electrons, (primaries plus secondaries) per primary, at any given kinetic energy T, the ordinate variable can be interpreted as a rough measure of the fraction of the input energy T_o which these electrons represent.

dominate in this region. Below $T_0 \approx 1$ keV the minimum tends to disappear. But the tendency of the spectra to converge keeps a value $\sim B^{-1}(.5\ \text{keV})$ significant to still lower energies. At the right of the figure, some of these values have been indicated.

A remarkable feature noted previously by Berger [34] is a strong tendency of the curves to converge at low energies, so that the shape of the slowing-down spectrum is nearly independent of T_0 in this region. One sees in eq (9') a tendency of this type in the $y^{(1)}$, since B varies slowly for large T_0. In higher generations of secondaries the upper limit of the integral on the right of eq (8) becomes largely irrelevant, so that one expects these components to depend on T_0 only through $B(T_0/2)$ at most. But the convergence seen in fig. 7 is more striking than this and must reflect further restrictions imposed by energy conservation. Table 3 illustrates this strong trend towards T_0-independence of the low energy components. Convergence is evidently according to a trend somewhat of the type

$$y(T,T_0) \sim y(T,\infty) + \alpha_0/\log(T_0/\alpha_1) \quad , \tag{10}$$

where α_0, α_1 depend on T only, because equal factors of increase in source energy improve convergence by comparable increments.

D. The ionization yield

Because degradation spectra have extensive applications to the evaluation of excitation and ionization yields, we turn to the discussion of the ionization yield, usually given in terms of a quantity W, eV per ion pair,

$$W^{-1} = T_0^{-1} \int_0^{T_0} dT\ k_i(T)\ y(T,T_0) \quad ,$$

where k_i is probability for ionization per unit path length by electrons with kinetic energy T. At the bottom of fig. 7 a curve of K_i/S has been

included. It is instructive to consider the different contributions to the value of W^{-1} for H_2. The T/T_o trend of fig. 7 for the primaries, which follows from CSDA, has the consequence that the contribution by primaries can be approximated by evaluating (k_i/S) at the midpoint energy $T_o/2$, e.g., .018 for T_o = 30 keV. Correspondingly, the fact that both (k_i/S) and $(T/T_o)Sy$ are comparatively flat means that a rough evaluation of the contribution due to secondaries can be obtained with similar ease. One notes that large contributions, say in the case of 30 keV, occur between ~ 20 eV, and ~ 2500 eV. The midpoint of this range (in the logarithm) is $(20 \times 2500)^{\frac{1}{2}}$ = 224 eV. Evaluation of both K_i/S and $(T/T_o)Sy$ curves at this energy, with the product multiplied by $\ell n(2500/20) = 4.83$ gives a value .0095. We thus estimate that $W \approx 1/(.018 + .0095) \approx 36.4$ eV. This agrees rather well with more accurate calculations.

One can see from these curves that the high energy gradual decrease of k_i/S will decrease the contribution to W^{-1} due to primaries, as the source energy T_o is raised. On the other hand, secondary electron contributions will increase. Unfortunately, the resulting rough cancellation of competing effects provides no simple explanation for the impressive T_o-independence found in experimental investigations of W.[6] But this approach could probably be developed to give rough estimates fairly readily.

Pursuing the question of W further, we present values due to other investigators in table 4, and for different source energies in table 5. A minimum occurs in the vicinity of 2 keV, with a very slow rise with increasing source energy. Comparisons with results from experiments and other recent

---

[6] See refs (7) and (8) for an interesting approach to this problem which uses scaling of the slowing-down spectra.

computations are very interesting, and are displayed in figs. 8 and 9. In fig. 9 one sees that Garvey, Porter, and Green (GPG) obtain a much larger rate of increase in W with source energy above ~ 3 keV. On the other hand, in fig. 8 the data of GPG show a more rapid increase of W as T_o is decreased from 3 keV to below 200 eV. We have not attempted to analyze these differences in detail; but analogous differences in the case of H_2O can apparently be traced to differences of cross section. One need not assume that computational procedures are the cause of such contrasting trends.

The case is different in the comparison with Gerhart shown in fig. 8. While the cross sections used in our calculations are not identical with those of Gerhart, the differences would not seem to be sufficiently great to give rise to the $\sim 10\%$ differences in W which occur.

In fig. 8, the dashed line gives values of W inferred from the following formula, which depends on the ratio of total to ionization cross sections:

$$W = T_o \frac{\sigma_{tot}(T_o)}{\sigma_{ion}(T_o)} \quad , \tag{11}$$

As discussed by Jones [51], such an expression is valid when one ionization is energetically possible, but two interactions of which at least one is an ionization are not possible. This condition applies below about 26 eV for the case of H_2. The bump shown in the W curve is therefore a consequence of cross section ratios and does not follow from multiple processes. Experimental values due to Combecher [57] do not show this reversal clearly, although they exhibit a shoulder at corresponding energies. Such reversals have been reported in references [23,58,22], and also by D. Douthat [54]. We do not know whether this is a real phenomenon or not. It is strongly dependent on cross sections which are not well known as yet.

Equation (11) furnishes a good monitor for the accuracy of the slowing-down computations, since corresponding values can be obtained by application of the computer programs, which were designed for much greater source energies and are therefore put to a hard test at low energies. Agreement shown in fig. 8 thus constitutes a good check.

Figure 10 gives a different plot of some of the data of fig. 8. Below ~ 27 eV, the solid curve represents the cross section ratio of eq (11). Below 20 eV Combecher's data differs by a factor ~ 1.2 in magnitude from the solid curve; and by inference from eq (11), this difference measures differences of cross sections. Since our calculations thus appear to permit too much ionization at low energies our W values may be somewhat low at high energies. But this same argument means that Douthat's two versions of cross sections below 100 eV should give rather different W values at high energies.[7] In our experience, high energy W values are rather sensitive to low energy cross sections, even those below 25 eV.

It may be that the rather reasonable values for W obtained here occur because Gerhart's cross sections for ionization are too large at low energies, as evidenced by Combecher, but are correspondingly too small at high energies, as much other data suggests.

Figure 11 compares our slowing-down spectra for T_0 = 10 keV with corresponding spectra due to Douthat [1] and GPG [2], as read from the published curves. In a general way, our values lie between those of the other authors, with the largest differences occurring at low energies, where factors of 2 can be seen. For the region above ~ 300 eV, which is dominated by $y \approx S^{-1}$, the agreement is generally good, as can be expected.

---

[7] Douthat's lower values, ⊕ in fig. 7, correspond to a cross section set rather similar to ours. His higher values, +, correspond to about a 28% reduction in excitation cross section with ~ 16% increase in ionization cross sections.

Table 6 gives a few comparisons with data for T_o = 100 keV due to Okazaki and Sato [15]. No agreement is evident even at high energies where the y values depend essentially on the stopping power alone.

Appendix I. Cross Section Data

For purposes of constructing a computer program for the integration, we have used a well-known set of cross sections, viz the H_2 cross section set developed by Donald E. Gerhart for his PhD thesis [3], even though there are some unsatisfactory aspects to them. In this appendix we describe necessary modifications and adaptations.

Gerhart uses Platzman's approach, which depends on the Williams-Weiszäcker approximation in which the passage of a fast charged particle is replaced by a nearly equivalent spectrum of virtual photons, which are subject to photo-electric absorption [84]. Collisions are classified as either "glancing" or "knock-on." Glancing collisions, with small momentum transfer, are assumed to follow expressions derived for zero momentum transfer. Knock-on collisions are assumed to follow cross section forms based on collisions between free electrons.

A. Glancing Collisions (Small momentum transfer, large impact parameter).

First, in regards to excitations due to glancing collisions we follow Gerhart in the use of the Bethe excitation cross section formula as follows:

$$\sigma_n = \frac{4\pi a_o^2 R}{T} \frac{f_n}{E_n/R} \ln\left(\frac{4T}{R} c_{set}\right) , \qquad (I.1)$$

where $R = 13.6$ eV and f_n is the oscillator strength for the n'th transition of a set, which can be any group of transitions treated together. The constant c_{set} in the logarithm, which in principle differs from transition to transition, is assigned an average value appropriate to a set of related lines such as those constituting the Lyman or Werner bands of H_2.

Ionizations due to glancing collisions are described by the analogous cross section form

$$\sigma_i = \frac{4\pi a_o^2 R}{T} \frac{\eta_i(E)}{E/R} \frac{df}{dE} \ln\left(\frac{4T}{R} bR^2/E^2\right) , \qquad (I.2)$$

where η_i is an "ionization efficiency" function, and b is essentially the reciprocal of an impact parameter in a_o units, or a cut-off for the square of the momentum transfer in glancing collisions. The variable E is the transition energy, and df/dE is the differential oscillator strength distribution (OSD).

The OSD developed by Gerhart is based largely on discrete excitation data due to Allison and Dalgarno [59] and experimental data due to Cook and Metzger [60], both modified to satisfy information from sum rules. The important and complex far-ultraviolet region from 14.4 to 16.5 eV is described by replacing the discrete Rydberg states with a carefully estimated continuous extension of the continuous part of the OSD at higher energies.

The f_n data of Table I.1 are from Gerhart, and represent his modification of the data due to Allison and Dalgarno. The corresponding E_n data were not given nor referred to in [3]; they are due to Namioka [29].

The ionization efficiency function η_i used by Gerhart is reproduced from his paper in fig I.1. A dash-dot line, corresponding to an analytic approximating function

$$\eta_i(E) \approx 1. - \left(\frac{15.4}{E}\right)^{30.8} \qquad (I.3)$$

has been added; we used this curve for convenience, despite the fact that it can clearly be improved.

The mathematical form of eq (I.1) is a discrete analog of eq (I.2). In both cases, the expression can be written as the sum of two products, each having a function $f(T)$ multiplied by a function $g(E)$ (or g_n) of the transition energy. We proceed to a unified treatment of excitations and

ionizations in which cumulative integrals (or sums), extend from zero transition energy over excitations and then ionizations, up to a maximum energy of about 220 eV. Three such cumulative integrals (f_n, $\frac{df}{dE}$ multiplied by factors E_n^i or E^i, $i = 0,1,2$), are tabulated at intervals of about 0.4 eV for small transition energies, with the interval size increasing geometrically with E. A second set of integrals includes a factor $\ell n(E_n)$ or $\ell n(E)$. The resulting 6 tabulations are given in Table I.2. The first three columns ($\mathcal{L}$) are energy moments of f_n and $\frac{df}{dE}$ while the latter three columns ($\mathcal{S}$) are energy moments of $f_n \ell n(E_n)$ and $\frac{df}{dE} \ell n(E)$, E_n and E in eV. Factors $(1 - \eta_i)$ and η_i are included in calculations for excitations and ionizations, respectively. These tables form the numerical basis for all computations involving glancing collisions.

The use of three integrals, yielding three moments of the transition energy, has the following significance: The zeroth momenth is essential to the evaluation of the total cross section; the first moment is required for stopping power calculations; and by use of three moments one may perform Gauss quadrature calculations of quadratic accuracy.[1]

The constant b was assigned a value 2.3 by Gerhart. As will be discussed in section C below, we found it convenient to make b a function $b(T)$ for electron kinetic energies T below 707 eV.

We note that eqs (I.1) and (I.2) are non-relativistic and require modification to achieve the relativistic forms. This is essential because we wish to do calculations at relativistic as well as non-relativistic energies. Hence we modified all glancing cross sections by replacing the logarithmic factor $\ln(4T/R)$ as follows:

---

[1]The second moment is important in straggling theory.

$$\ell n \left(\frac{4T}{R}\right) \rightarrow \ell n \left[2 \frac{T}{R} (T^* + 2)\right] - \frac{T^*(T^*+2)}{(T^*+1)^2} \quad , \qquad (I.4)$$

Where $T^* = (T/mc^2)$ and the term on the right is the square of the velocity, $\beta^2 = (v/c)^2$. Likewise, the factor (R/T) appearing at the left of cross section forms given in eqs (I.1) and (I.2) was replaced by $2(R/mc^2)\beta^{-2}$.

B. Knock-on Collisions (large momentum transfer, small impact parameter).

Gerhart also made use of non-relativistic forms for the knock-on cross section. These he multiplied by a factor $\phi(E)$ and by another factor $C(T)$. The latter factor, which was evidently introduced to improve agreement with total cross sections below $\sim$ 1000 eV, makes it impossible to derive the Bethe stopping power formula without some change in Gerhart's formulae. Hence we simply eliminate $C(T)$ by equating it to unity. This leaves us with Gerhart's problem of obtaining agreement with data on total cross sections below 1 keV, and this is discussed in the next section.

Gerhart's function $\phi(E)$ was introduced as a smooth cut-off to the spectrum of transition energies resulting from the knock-on process. $\phi(E)$ is shown in fig. I.2, together with a simple step-function approximation which assumes zero cross section for $E < 17.5$ eV, which we decided to use. In our opinion, the slowing-down spectra are not sensitive to such a change of shape; and the sharp cut-off simplified both numerical and analytic procedures.

Consistent with the point of view already expressed, we use the fully-relativistic Møller cross section to represent the knock-on process, modified in a simple way to take account of a mean energy $I \approx 16$ eV for ionization:

$$\sigma_{ko} = \frac{8\pi a_o^2 R^2 Z}{\beta^2 (mc^2)} \left\{ \frac{1}{E^2} + \frac{1}{(T+I-E)^2} - \frac{(2T+mc^2)}{T(T+mc^2)^2} mc^2 \left(\frac{1}{E} + \frac{1}{T+I-E} \right) \right.$$

$$\left. + \frac{1}{(T+mc^2)^2} \right\} u(E-17.5) \quad , \tag{I.5}$$

where the unit function, $u(x) = \begin{matrix} 1, & x \geqslant 1, \\ 0, & x < 1, \end{matrix}$ expresses the cut-off shown in fig. I.2 for low energy excitations by this process.

C. Low energy ionization cross sections.

Gerhart chose to use a simple E^{-2} cross section for all processes at low energies, i.e., $T \leqslant 300$ eV. This function was normalized to give a value for the total ionization cross section in agreement with experimental data due to Rapp and Englander-Golden (REG) [33]. We have chosen a different approach to the problem of the selection of differential cross sections at low energies: we continue to use eq (I.2), but assign to b (for $T \leqslant 707$ eV) an energy dependence $b(T)$ adjusted to give total cross sections in agreement with REG. The theoretical basis for the T-independence of b breaks down at low energies. In fact, since there is no theoretical basis at low energies for the asymptotic form which we use, this procedure should be considered only as an ad hoc extrapolation guided by an experimentally fixed integral. Incidentally, Miller used $b = b(E)$ [58], but there is some theoretical justification for this [62]. Even so, as the glancing component decreases in importance at low T, it is not unreasonable to assign this to a decreasing range of contributing momentum transfers.

Use of values for $b(T)$ as large as $b = 3$ at $T = 1$ keV could accomplish essentially the same thing as Gerhart's $C(T)$ although we have not incorporated this adjustment; while for $T < 500$ eV use of $b(T)$ results in

more gradual change of spectrum than that due to Gerhart's prescription. Table I.3 gives $\ell n[b(T)]$ values which we have used. Table I.4 shows the comparison with REG thus attained.

Our approach is no less arbitrary than that adopted by Gerhart and in modified form by Douthat. Our value for b above 707 eV is 2.34. This sacrifices close agreement with REG in the region 707 eV < T < 1000 eV, but preserves the asymptotic agreement of stopping powers at high energy with the Bethe stopping powers based on a value for the mean excitation potential consistent with Gerhart's OSD.

D. Low energy excitation cross sections

Figures 9 and 10 of Gerhart's paper [3] present his "adopted" electron impact cross sections. Since our purpose here is to perform electron slowing-down calculations with minimal changes in Gerhart's cross section set, we have reduced these curves to tabular form for our use, with no significant modifications. But one should note that accurate values in the important energy region 13 eV < T < 25 eV cannot be obtained in this way, and detailed features of the spectra in this region can be wholly spurious.

These total cross section data must be in some manner complemented with information about associated transition energies. In the case of the Lyman and Werner discrete excitations one has values for individual transition energies [29]; but for higher energy excitations a range of energies from approximately 14.4 eV to 17 eV is involved, with the use of a continuous OSD function in place of the actual complex line structure as already noted. Our first approach was to choose for each process separately a functional form of the type

$$[1 - \eta_i(E)] \frac{R}{E} \frac{df}{dE} \ell n\left(4 \frac{T}{R} b(T)\, c_{set}\right) \quad . \tag{I.6}$$

But since the slowing-down calculation depends for the most part only on three moments (integrals) over the transition energy, we carried use of this form a step further and applied it to the combination of all excitation cross sections. This leads to slightly different values $b_j(T)$, $j = 1,2,3$, for the three different moments, as required to agree with calculations having different $b(T)$ values for different processes as in eq (I.6). However, it turned out that these b_j differed in a regular manner, but only by $\sim 1\%$. Hence we eventually used only $b_1(T)$, which was assigned values very slightly larger than those calculated from total cross section data. Tabulated data for resulting b_1 function are given in Table I.3; and a comparison of resulting total cross section values to those of Gerhart is given in Table I.4.

The full differential spectrum is important when single interactions are significant. We calculated these spectra by use of eqs (I.2) and (I.6), using values for $\ell n(b)$ and $\ell n(b_1)$ already described. Figures 1 and 2 give some results of these calculations.

Vibrational effects become important below about 20 eV; and they constitute the main part of the cross section below the lowest electronic transition energy, here taken to be 11.213 eV. Though ignored by Gerhart, we have included them on the basis of data by Ehrhardt et al. [63] and Trajmar et al. [64]. We use only two excitation energies, 0.54 eV and 1.08 eV. For electrons with kinetic energy greater than 20 eV, we use the following simple expressions for the (non-relativistic) differential cross sections:

$$k_1/\kappa \approx [- .00457 + .00588\ \ell n(4T/R)]\ \delta(E - .54) \quad , \qquad (I.7)$$

$$k_2/\kappa \approx [- .000309 + .000287\ \ell n(4T/R)]\ \delta(E - 1.08) \quad , \qquad (I.8)$$

where $\kappa = 4\pi a_0^2 R/T$. Below 20 eV, we tabulated the total cross section data and perform interpolations as required. Tabular data are recorded in Table I.5; these are a somewhat smoothed version of the data in Ehrhardt et al and Trajmar et al.

The experimental data do not extend beyond 80 eV; hence the use of eqs (I.7) and (I.8) for much higher energies is not necessarily accurate. But because the contribution is a small one, this extrapolation was used (with the relativistic modifications.) Equations (I.7) and (I.8) are of the type which can be readily incorporated into the subroutine OSCUM which evaluates differential and integral total oscillator strengths. But we prefer to treat vibrations by use of separate computations which could be used or not as desired.

E. Symmetry of glancing collision cross sections

One problem which must be solved to preserve energy conservation at low energies is the following: In the case of glancing collisions, for which the cross sections are not written symmetrically, secondary electrons with kinetic energy (E - I) are generated with the same probability as that corresponding to energy losses E. A type of symmetrizing is necessary in order to guarantee this feature. We chose to accomplish this by terminating the cross sections at an energy loss for which secondary and primary electrons had equal kinetic energy, and then repeating the cross section structure below this energy so that it has identical values for kinetic energies equally above and below that value at which primary and secondary kinetic energies coincide. This seems a little easier than the alternative approach of adding a symmetrizing term. Where the difference between approaches is significant, we

feel that the effect on the spectrum is small, so that any improvement would call for evaluation of more accurate and properly symmetrized cross sections, i.e., a major effort.

F. The mean excitation potential

A mean excitation potential $\langle I \rangle_B$ can be determined for the oscillator strength distribution for use in Bethe's stopping power formula [65]:

$$\langle I \rangle_B = 2\ R\ \exp\left\{Z^{-1} \int_0^Z df\ \ell n\ (E/2R)\right\} . \qquad (I.9)$$

Analogously, cross sections which we have adopted lead to a high energy stopping power of Bethe's form; and if we determine an equivalent parameter $\langle I \rangle_P$ (P for Platzman) we find the following expression:

$$\langle I \rangle_P = 2R\ \exp\left\{Z^{-1}\left[\int_{\text{ioniz.}} df\ \ell n\ \frac{E}{\sqrt{b}R} + \sum_{\text{sets}} \sum_n f_n^{\text{set}}\ \ell n(1/\sqrt{c}_{\text{set}}) + \frac{Z}{2}\ \ell n\left(\frac{I_c}{4R}\right)\right]\right\} \qquad (I.10)$$

where I_c is a cut-off for low energy knock-on collisions, which was assigned the value 17.5 eV to correspond to Gerhart's cut-off function $\phi(E)$.

Table I.6 gives values for $\langle I \rangle_B$ and $\langle I \rangle_P$, in comparison with values by other authors. Consistency between $\langle I \rangle_B$ and $\langle I \rangle_P$ can be improved, but it is interesting that $\langle I \rangle_B$ agrees rather well with other theoretical estimates, while $\langle I \rangle_P$ is consistent with experimental values. Partly for this reason we have not enforced agreement between $\langle I \rangle_B$ and $\langle I \rangle_P$.

APPENDIX II. Description of the Subprograms constituting ELSPEL

The descriptions which follow are in the order shown in table II.1, proceeding from differential to integral cross sections, to the subprograms guiding the solution.

A. Elementary Cross Section Subroutines

1. OSCUM(E,ISET,ID)

The output from this subroutine consists either of cumulative integrals over the oscillator strength (OS) distribution (ID = 0), or the differential distribution itself (ID = 1). The six cumulative integrals (for ionization) are as follows: (R = 13.6 eV)

$$\mathcal{S}_m^i = \int_0^{\Delta E} dE\ (E/R)^{m-1}\ \frac{df}{dE}\ \eta_i(E),\ m = 0,1,2, \tag{II.1}$$

$$\mathcal{L}_m^i = \int_0^{\Delta E} dE\ (E/R)^{m-1}\ \ell n(E)\frac{df}{dE}\ \eta_i(E),\ m = 0,1,2,$$

where E is in eV in the factor $\ell n(E)$.

For excitations the corresponding quantities are, ($E_n \in \Delta E$) and m = 0,1,2,

$$\mathcal{S}_m^e = \sum_{sets} \sum_n (E_n/R)^{m-1}\ f_n^{set}\ [1 - \eta_i(E_n)]\ , \tag{II.2}$$

$$\mathcal{L}_m^e = \sum_{sets} \ell n(1/c_{set}) \sum_n (E_n/R)^{m-1}\ f_n^{set}\ [1 - \eta_i(E_n)]\ ,$$

where the distinct "sets" include Lyman, Werner, excitations with principle quantum number $n = 3$, and the combination of all other excitations involving transition energies between 14.2 eV and 16 eV. But we reduce these four types of interaction to three in practice because the OS distribution, which is taken to be effectively continuous in this energy region, is treated in Gerhart's paper as identically the same in shape for all excitations which are neither Lyman nor Werner [3].

Cumulative integrals over excitation oscillator strength appear in an output array ASRE(I), where $I = 1,2,3$ correspond to $m = 0,1,2$ of the $\mathcal{S}_m^e$ integrals of eqs (II.2), and $I = 4,5,6$ relate to the corresponding $\mathcal{L}_m^e$ integrals of eqs (II.2). Similarly, for ionizations the output is in ASRI(I), where index values $I = 1,2,3$ correspond to the first integrals of eqs (II.1); and index values $I = 4,5,6$ correspond to the integrals of eqs (II.1) containing the logarithmic factor.

For $ID = 1$ and $E \geq 17$ eV, the value of df/dE for ionizations appears in ASRI(1), while $\ell n(E)df/dE$ appears in ASRI(2). For $E < 17$ eV, equivalent quantities are obtained by differencing the cumulative tabulations; these appear in ASRE(1), ASRE(2), ASRI(1), and ASRI(2), the index 2 referring to the quantity with the logarithmic factor. (These equivalent quantities are $\Delta\mathcal{S}_0^e$ and $\Delta\mathcal{L}_0^e$ divided by the width ΔE for any interval.) Note that for the $ID = 1$ case, the output has units $(eV)^{-1}$.

Input tabulations for OSCUM are read from cards, when $ISET \neq 1976$. One set of input data (EON, for ionizations) consists of cumulative integrals tabulated at intervals from 15.176 eV to 17 eV. The other set (EXC, for excitations) is a similar tabulation extending from 11.213 eV to 17 eV. The two tabulations are listed in table I.2. Corresponding energies are read into EOS.

The method for computing ASRE and ASRI values is interpolation on the prepared tables. For our calculations, based on Gerhart's set of cross sections, the following forms were used to extend the tables to 222.7 eV, where E values are in eV:

transition energy (list name: EOS):

$$E_n = E_{n-1} \, (17/11.213)^{1/11}, \quad n = 1, \ldots, 80 \qquad \text{(II.3)}$$

excitations and ionizations, 14.2 eV to 17 eV (list name: EXC):

$$df/dE \approx \frac{20.3}{E^{1.85}} \quad , \qquad \text{(II.4)}$$

ionization efficiency:

$$\eta_i \approx 1 - \left(\frac{15.4}{E}\right)^{30.8} \quad , \qquad \text{(II.5)}$$

ionizations (list name: EON), 17 - 35 eV:

$$\frac{df}{dE} \approx \frac{275}{E^{2.77}} \quad , \qquad \text{(II.6)}$$

for 35 eV to 222.7 eV:

$$\frac{df}{dE} \approx \frac{1624}{E^{3.27}} \quad , \qquad \text{(II.7)}$$

for $E > 222.7$ eV

$$\frac{df}{dE} = 0 \quad . \qquad \text{(II.8)}$$

Interpolation requires both positioning on the table, and an interpolation formula. Positioning was accomplished as follows by determining the equivalent index by the formula below, where N is the next integer below EX:

$$EX = \frac{\log(E/11.213)}{(1/11)\log(17/11.213)} + 1 \quad , \tag{II.9}$$

$$N \leqslant EX \quad . \tag{II.9'}$$

The interpolation weights could then be calculated from (EX - N), with integer separation between tabulated abscissa values. A simple 3-point rule was used for this purpose.

The df/dE tabular values were obtained as previously mentioned by differencing as follows in the region below 17 eV:

$$\frac{EON(I,J+1) - EON(I,J)}{EOS(J+1) - EOS(J)} \quad ,$$

$$\frac{EXC(I,J+1) - EXC(I,J)}{EOS(J+1) - EOS(J)} \quad , \quad \text{for } I = 1,4 \text{ and } 1 \leqslant J \leqslant 12. \tag{II.10}$$

No attempt was made to apply interpolation for $E < 17$ eV when df/dE was required; a histogram structure was assumed. Interpolations were, however, used for ionization above 17 eV.

2. VIB(T,ARGL,X1,X2)

Output for this subroutine are values for the total vibrational cross sections at kinetic energy T, for 1st and 2nd excitation levels; these values are designated X1 and X2, respectively. for energies greater than T = 20 eV, the values X1, X2 are given by formulae as follows:

$$X1 = - .00457 + .00588 * ARGL$$

$$X2 = - .000309 + .000287 * ARGL, \qquad (II.11)$$

where the constants $.00588 \cdot (.54/R)$ and $.000287 \cdot (1.08/R)$ are oscillator strengths for the two transitions.

In addition to the input parameter

$$ARGL = \ell n[2(T/R)(2 + T/mc^2)] - \beta^2(T) \quad , \qquad (II.12)$$

an input table VB for each level is read from cards, as is a corresponding tabulation of the quantity $\ell n(4T/R)$, which is stored in the list TVB.

For energies less than 20 eV, the method used is an interpolation, by means of 3-point weights. Positioning on the TVB table for a calculation at $T = T_a$ is accomplished by a search for the lowest tabular value exceeded by $U = \ell n(4T_a/R)$.

Data on which the linear forms (for $T > 20$ eV) are based do not extend above 80 eV; hence the constants used are probably not very accurate at higher energies. But the cross sections are small at high energies, so that this is not important.

3. BMOD(T,B1)

The output value of this function routine is B1 and

$$BMOD = \ell n(b_\infty/b) \quad , \qquad (II.13)$$

where $b = b(T)$ is the momentum parameter which separates glancing from knock-on collisions. For the tabulation we have taken $b = b_\infty$ for

$T > (1000)\sqrt{2}$ eV, and have used $b_\infty \approx 3$. For lower electron kinetic energies, the value of $b(T)$ has been chosen to render a total cross section for ionization in agreement with experiment (Rapp, Englander-Golden [29]). But in practice we modify this to $\ell n(b_\infty/b) = .25$ for $T > 707$ eV, and b_∞ correspondingly equals 2.34.

The parameter B1 is defined similarly,

$$B1 = \ell n[b_1(\infty)/b_1] \tag{II.14}$$

where $b_1(\infty) = 1$, a value which applies for $T \gtrsim 350$ eV, as shown in Table I.3. This parameter corrects the total cross sections to agree with low energy values, as discussed in section 3(D).

Input consists of a tabulation of values for $\ell n(b_\infty/b)$ and $\ell n[b_1(\infty)/b_1]$, which are read from cards into the lists BCOR(I,1) and BCOR(I,2), respectively. Data are given in Table I.3.

Method of evaluation is interpolation on the table. Between 15.62 eV and 707 eV, 2-point trapezoidal rule interpolation is used. Below 15.62 eV, a 3-point rule is used instead. Positioning on the table is accomplished as in OSCUM, viz. for N equaling the integer just less than X,

$$X = \frac{\log(1000/T)}{\log\sqrt{2}} + 2 \quad ,$$

$$N \lesssim X \quad . \tag{II.15}$$

An extra point has been inserted at low energies in each list to give greater accuracy near threshold.

4. DTU(T,B,TB)

Output of this function routine are two numbers, DTU and TB. Both relate to maximum transition energy for glancing ionizations. For a given value of T, and corresponding cut-off b(T), DTU is the maximum allowed energy for glancing ionization transitions from higher kinetic energies to I. Correspondingly, TB is the least kinetic energy for electrons capable of giving rise to the transition energy (T + I), where T is the kinetic energy of secondary electrons and I = 16 eV is a mean ionization energy for molecular hydrogen. Thus DTU relates to the energy loss of primaries, and TB to the energy of secondaries; both express glancing collision limits.

In addition to T and $B = \ell n(b_\infty/b(T))$, this subroutine requires BMOD, because both DTU and TB are evaluated by reverse interpolation to solve the transcendental equations

$$2T^* \, Rb(T^*) \left(2 + \frac{T^*}{mc^2}\right) \exp[-\beta^2(T^*)] = (DTU)^2, \; T^* = T + DTU \quad , \tag{II.16}$$

$$2T^* \, Rb(T^*) \left(2 + \frac{T^*}{mc^2}\right) \exp[-\beta^2(T^*)] = (T + I)^2 \quad , \quad T^* = TB \quad .$$

The reverse interpolation is based on a list of energies

$$RAD(I,1) = 9(2^{1/6})^{I-1} \text{ eV}, \tag{II.17}$$

and a corresponding tabulation RAD(I,2) of values for the square root of the left side of the transcendental equations above, when values of the energy list RAD(I,1) are equated to T^*.

The positioning is accomplished by a search to locate both $(T^* - T)$ and $(T + I)$ in the list RAD(I,2), treated as abscissa list. A 3-point interpolation is then applied to RAD(I,1), treated as the ordinate list, to find the value of T^* corresponding more exactly to $(T^* - T)$ and $(T + I)$ than the neighboring tabulated values of RAD(I,2). This T^* then gives the output, directly in the case of TB, and through use with $(T^* - T)$ in the case of DTU.

This rather lengthy positioning operation would probably take too much time if DTU and TB values were required throughout, rather than for the list of solution energies only, i.e., a linear set of no more than 100 to 200 values.

B. Combined Cross Section Functions

5. TCX(T,DT,IVB)

Output of this function routine is a quantity which can be considered as either (for non-relativistic energies) total cross section times $\frac{mc^2}{Z}(T/4\pi a_o^2 R^2)$ or total interaction probability divided by XKAP (as defined below), for all processes at kinetic energy T, integrated over energy transitions up to DT. For $DT \geq (T + 1)/2$, the value of TCX is the total cross section. In addition, this subroutine calculates certain partial cross sections, as follows:

XKAP: This is the function which multiplies the stopping or cross section number, to give interaction probabilities, in units (cm^2/g). That is, $XKAP = \frac{3}{4}(N_A/A)\,\phi_o\, Z/\beta^2$, where ϕ_o is the Thomson cross section and $\beta = v/c$.

TGE: This is the glancing component due to electronic excitations (i.e., not including vibrations.)

TBI: This is that part of the glancing component for ionizations which has as a factor the cut-off parameter $\ell n[b(T)]$.

Input to this function routine is the value of BRSQ = $\ell n(b_\infty R^2)$, and, through reference to BMOD, the correction term $\ell n[b_\infty/b(T)]$. For IVB = 1, vibrational components are included while for IVB = 0 they are ignored.

The basic method involves use of OSCUM to determine the total relevant oscillator strength. To this component is added the knock-on contribution, and, depending on IVB, the contribution due to vibrational excitations.

Note that for very small T, i.e., below I = 16 eV, the value of DT can meaningfully exceed (T + I)/2, which becomes inoperable as a limit. Note also that the contributing glancing transition energies are not allowed to exceed a value TST, beyond which the glancing cross section is negative.

Equations (I.1) to (I.8) in Appendix I give formulae by which the cross sections are computed. We repeat below, using some of the computer terms, the important expressions and definitions for the cross section functions. Quantities used in calculations of glancing collisions are as follows, with $U = T/mc^2$, I = 1,2,3:

$$\text{ARGL} = \log\left[\frac{2T}{R}(2 + U)\right] - \frac{U(U+2)}{(U+1)^2} \quad , \tag{II.18}$$

$$\text{ASRI}(I) = \int_0^{DT} dE\left(\frac{R}{E}\right)^{2-I} n_i \frac{df}{dE} \quad , \tag{II.19}$$

$$\text{ASRI}(3+I) = \int_0^{DT} dE\left(\frac{R}{E}\right)^{2-I} n_i \frac{df}{dE} \ell n\, E \quad , \tag{II.20}$$

$$\mathrm{ASRE}(I) = \sum_{\text{all sets}} \sum_{E_n<DT} (R/E_n)^{2-I} f_n^{set} (1 - n_i) \quad , \tag{II.21}$$

$$\mathrm{ASRE}(3+I) = \sum_{\text{all sets}} \sum_{E_n<DT} (R/E_n)^{2-I} f_n^{set} \log(1/c_{set}) (1 - n_i) \quad , \tag{II.22}$$

where the summations over n are accomplished by integration for $E > 14.2$ eV. Calculation of the knock-on contribution uses the following moments of the Møller function:

$$(\epsilon_m = 16/mc^2, \quad \epsilon = E/mc^2, \quad U = T/mc^2, \quad \epsilon_c = 17.5/mc^2) \quad ,$$

$$\int_{\epsilon_c}^{DT} d\epsilon \; \epsilon^{I-1} \left[\frac{1}{\epsilon^2} + \frac{1}{(T+\epsilon_m-\epsilon)^2} - \frac{2U+1}{U(U+1)^2} \left(\frac{1}{\epsilon} + \frac{1}{T+\epsilon_m-\epsilon} \right) + \frac{1}{(U+1)^2} \right] . \tag{II.23}$$

In the case of TCX and TCXI, $I = 1$, while for STN, $I = 2$, in eqs (II.19) to (II.23).

6. TCXI(T,DT,GLI)

Output of this function routine is the interaction probability at kinetic energy T for all ionizing processes, integrated over energy transitions up to DT. For $DT \geqslant (T + I)/2$, the value of TCXI is the total cross section for ionization. In the computation of this quantity, however, the glancing and knock-on processes are separately calculated and can in principle be referred to separately. The argument GLI gives the glancing component.

Input for this function routine, and the method of calculation are the same as for TCX.

7. STN(T,DT,ISG)

Output of this function routine is the stopping "number" S/XKAP for all processes at kinetic energy T, integrated over energy transitions up to the limit DT. For $DT \geq (T + I)/2$, the value of STN is the total stopping number. The index ISG is assigned either the value 0 or the value 1: when $DT < (T + I)/2$, both glancing and knock-on ionizing transitions dissipate a mean energy I = 16 eV to atomic systems with each such interaction which occurs. In a general way, this additional dissipation should be included in STN when DT is used to identify "energy loss"; but this dissipation component should not be included in STN whenever DT is used to refer to (T + I), i.e., the rate of energy loss due to formation of secondary electrons. In the latter case DT is then usually associated with the maximum kinetic energy of secondary electrons under consideration; hence electrons with greater kinetic energies are not to be considered at all.

The value of ISG is irrelevant when total stopping number is being computed, i.e., for $DT \geq (T + I)/2$. Otherwise ISG = 1 signals inclusion of the extra component, while ISG = 0 refers to its exclusion.

Input for this function routine is the same as in the case of TCX, and the method of computation is essentially the same, except that different integrals (identified by I = 2) over the transition energy are used as indicated in the notes for TCX given previously.

8. ONCE(TP,DT,XKD,IX)

Output of this subroutine is $XKAP^{-1}$ times the differential cross section for various processes for electrons of kinetic energy TP undergoing energy loss DT. The output value is XKD. The value of IX relates to the inclusion or exclusion of secondary electrons: IX = 1 means that secondaries are included, while for IX = 0 or negative, secondaries are excluded.

Input into this subroutine is essentially the same as for TCX.

The calculation for glancing collisions utilizes OSCUM, in the mode (ID = 1) in which the differential OS value for excitations or ionizations below 17 eV is obtained by numerical differentiation. The differential OS values for higher energy transitions are obtained in OSCUM by interpolation on a predetermined list. Cross sections for knock-on collisions are given by Møller formula, with $\epsilon_m = 16/mc^2$, $\epsilon = E/mc^2$, $U = T/mc^2$:

$$\frac{1}{\epsilon^2} + \frac{1}{(T+\epsilon_m-\epsilon)^2} - \frac{2U+1}{U(U+1)^2}\left[\frac{1}{\epsilon} + \frac{1}{T+\epsilon_m-\epsilon}\right] + \frac{1}{(U+1)^2} \quad . \qquad \text{(II.24)}$$

One should note that the use of a limit (DT < TST) ensures evaluation of glancing collision cross sections only when they are positive. Also, for DT > (TP + I)/2, glancing collisions are calculated with (TP - DT) replacing DT, corresponding to an energy loss totaling I plus the energy of the secondary electron.

C. Subroutines for Evaluating the Scattering Integral

9. HARDP(N)

Output of this elementary tabulation subroutine is a list HKI(N,J) which is used in the evaluation of the scattering integral. Setting T = T(N), the n'th solution energy, the following values are currently included:

$$\begin{aligned}
&HKI(N,1) = ARGL = \ell n[2(T/R)(2 + T/mc^2] - \beta^2 \\
&HKI(N,2) = 1. \\
&HKI(N,3) = -\frac{(2T/mc^2+1)}{(T/mc^2)(1+T/mc^2)^2} \\
&HKI(N,4) = 1/(1 + T/mc^2)^2 = (1 - \beta^2) \\
&HKI(N,5) = \ell n(b_\infty/b) = BMOD \\
&HKI(N,6) = \ell n(1/b_1) \\
&HKI(N,7) = DTU \\
&HKI(N,8) = TB, \text{ as given in FUNCTION DTU.}
\end{aligned} \qquad \text{(II.25)}$$

These will all be recognized as functions of T required in cross section formulae. The first six are required sequentially in the order given above, in a DO-loop.

10. CUMK2(N,NP,A,B,C)

Output for this subroutine are integration weights A,B,C to be applied to $y(T_{NP+1},T_o)$, $y(T_{NP},T_o)$, and $y(T_{NP-1},T_o)$, respectively. These weights take account of both the energy region T_{NP} to T_N in the scattering integral and the "scatter-out" term $K(T_N)y(T_N,T_o)$ usually placed on the left side as in eq (1). Note that this region of the scattering integral is complicated and difficult; the three weights contain the contribution by the kernel function k(T',T), which has singular and irregular behavior for T' near T.

The weights are obtained by Gauss quadrature, using 3 moments and 3 Dirac delta functions except when NP = 1, in which case only 2 moments and Dirac delta functions are used. The general concept is described in section IV, C in the text. Basically, one is using eq (4) and making the approximation ($\Delta T_{NP} = T_{NP} - T_N$, etc.)

$$g_i(E) \approx \alpha_i \delta(E - \Delta T_{NP+1}) + \beta_i \delta(E - \Delta T_{NP}) + \gamma_i \delta(E - \Delta T_{NP-1}) \quad , \qquad (II.26)$$

such that

$$\int_0^{\Delta T_{NP}} dE\ E^j\ g_i(E) = \alpha_i \Delta T_{NP+1}^j + \beta_i \Delta T_{NP}^j + \gamma_i \Delta T_{NP-1}^j \quad . \qquad (II.27)$$

One then cumulates all terms, with the appropriate f_i factors:

$$WT(NP+1,N) = \sum_i \alpha_i f_i(T_N + \Delta T_{NP+1}) \quad ,$$

$$WT(NP,N) = \sum_i \beta_i f_i(TN + \Delta T_{NP}) \quad , \qquad \text{(II.28)}$$

$$WT(NP-1,N) = \sum_i \gamma_i f_i(T_N + \Delta T_{NP-1}) \quad .$$

We found it desirable to include the term $K(T_N)y(T_N,T_o)$ as a separate weight, $WT(N,N)$, when $NP + 1 \neq N$. But when $NP + 1 = N$, this term was incorporated into the integrand of eq (II.27) by use of the representation $K(T_N + E)\delta(E)$.

11. CUMK3(T,DT,IX)

Output for this subroutine is a set of numbers $GL(J)$, $J = 1,\ldots,6$, on which integration weights for the scattering integral are based. These numbers correspond to the following integrals:

$$GL(J) = \int_T^{T+DT} dE\ g_J(E) - \int_T^{\infty} dE\ g_J(E) \quad . \qquad \text{(II.29)}$$

The final term in eq (II.29), which is independent of DT and is included only for glancing interactions, always cancels because only differences between GL values appear in the weights. It is used to control round-off errors; note that for large DT the value of GL should vanish for glancing interactions. Further, DT can be very large, with very many integration points.

The value of IX determines whether or not a contribution due to secondary electrons is to be included. For IX = 1 they are included, while for IX ≦ 0 secondary electrons are excluded. In the case of knock-on interactions, this exclusion is effected by ensuring that for DT > (T + I), the upper limit in the above integral is (2T + I). In the case of glancing interactions, inclusion or exclusion of secondaries is a more complex problem because the cross section does not explicitly have a symmetric structure. For DT < (T + I) eq (II.29) gives the relevant (glancing interaction) integrals, while for DT > (T + I), i.e., for glancing secondaries, we include a contribution

$$g_J(T + I) \int_{2T+I}^{T+DT} dE \quad . \tag{II.30}$$

One should note however that in all the above, the limits of integration can be modified by the requirement that the cross section never be negative, a condition expressed through limits to the value of E. Thus the upper limit of the integral in eq (II.29) cannot exceed T + DTU, while the lower limit of the integral in eq (II.30) must be at least TB, as evaluated with the DTU function routine.

12. WATES(N,IX)

Output of this subroutine is a full set of weights for evaluation of the scattering integral at the N'th value of T in the solution list. The value IX = 1 means that these weights take account of secondary electrons, while for IX ≤ 0 secondary electrons are excluded.

Basic to this subroutine is the concept expressed in eq (9), the use of Stieltjes integration: values of G_i are given in the list GL(I) which

constitutes the output of CUMK3. These values must be turned into integration weights, after which the output of CUMK2 can be included.

The procedure used (see section IV, C) is a bit indirect. The assumption is made that the integrand, which is the product $f_i(T + E)\, y(T + E, T_o)$, is no more sharply varying than quadratic in an arbitrary variable u such that $u = -1, 0, 1$ at three successive points T_I, T_{I+1}, and T_{I+2}. At these same three points the basic integration variables G_i have values $G_i(1)$, $G_i(2)$, and $G_i(3)$. We then write

$$\int dG_i\ (f_i y) = \int du\ \frac{dG_i}{du}\ (f_i y) \quad . \tag{II.31}$$

We next fit $G_i(u)$ by a quadratic function of u, from which (dG_i/du) can be approximately evaluated:

$$G_i(u) = a + bu + cu^2 \quad ,$$

$$G_i(-1) = a - b + c \quad ,$$

$$\text{etc.} \tag{II.32}$$

Three-point integration weights can then be applied for evaluation of the integral. While this integration procedure may not appear so, it is exact if the basic assumption is obeyed, that $f_i y$ can be exactly represented by a quadratic function of the variable u.

As in the case of CUMK2, the cumulation over i values with the f_i factors, and combination of different weights for the same point must be carried out.

We should note that general 3-point or Simpson rule calculations are suitable to an odd number of points, whereas the scattering integral will involve odd and even numbers of points alternately. For cases in which an even number of points occurs, the interval from TY(1) to TY(2) is separately evaluated as follows: The procedure previously described is followed for points TY(1), TY(2), and TY(3), except that the integration over the variable u is taken only from -1 to 0. The resulting three weights are included with the same cumulations and factors already described.

The subroutine closes by calling CUMK2 and including weights for the final integral, including the "scatter-out" term.

13. CORRX(X,UI2,UI1,UI0,A,B,C)

Output of this small correction subroutine are three values A, B, and C, which are essentially differences between 3-point integration weights based on the assumption of a continuous integrand, and Gauss quadrature weights which can take account of a discontinuity in the same interval.

The three points of the integration interval are UI2, UI1, and UI0, in that order. The value of X falls somewhere in the interval, this being the location of the discontinuity, with X = 0 corresponding to UI2. Size of the discontinuity is I^{-2}, as shown in the sketch below:

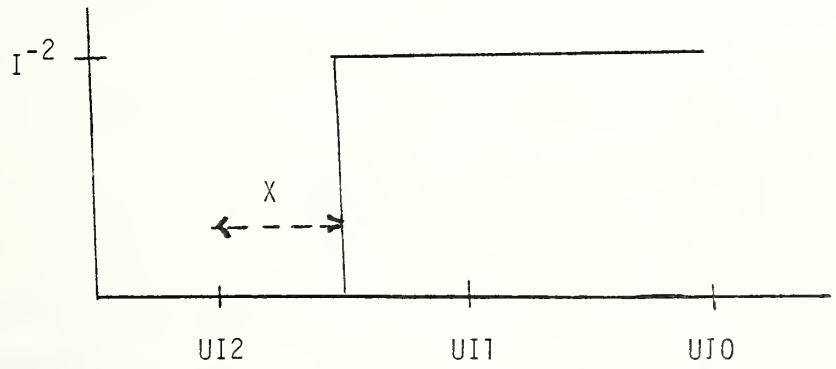

The function sketched is a constant times a unit function.

Such a discontinuity occurs in the differential knock-on cross section; and we take account only of the discontinuous part of the largest term, $E^{-2} = I^{-2}$, evaluated at the discontinuity. Integration as in CUMK3 here involves the variable (see eq. (4))

$$dG = 1\ dX\ , \tag{II.33}$$

and

$$\int du\ \frac{dG}{du}\ (f_i y)\quad . \tag{II.34}$$

The procedure used is that of constructing weights at the three points by straightforward application of three point numerical integration as discussed in WATES. But we also calculate weights by applying Gauss quadrature (in the variable X) to the step function by Dirac delta functions located at the three points indicated.

Differences between the two sets of weights give the values of A, B, and C.

The reason for this calculation is our impression that the Gauss quadrature approach is significantly more accurate for any interval containing the discontinuity generated at the 17.5 eV cut-off of the knock-on transitions.

D. General Evaluation of the Slowing-Down Spectra

14. TLIST(NPH)

Output of this subroutine is a solution list of energies, N3 in number, which are stored in the array TY(I). A peculiarity of this list is that for $T > T_0/2$, the quantity TY(I) corresponds to $(T_0 - T)$, while for $T < T_0/2$, TY(I) = T. The reason for this distinction is mostly the avoidance of round-off error in the computations.

The input constant NPH gives the factor by which T changes (in the intermediate energy region) between successive values, viz

$$T_o - T_n = (T_o - T_{n-1}) \cdot 2^{1/NPH} \quad . \tag{II.35}$$

The input constant N1 determines how many finely spaced intervals are utilized. These finely spaced intervals are separated approximately as the basic tabulations of OSCUM, and as given in an input list EOS. But the TY(I) are located between the EOS values according to the formula

$$TY(I) = \{EOS(I) \cdot EOS(I + 1)\}^{\frac{1}{2}} \quad . \tag{II.36}$$

After N1 of these values, two buffer intervals of 10 eV are inserted separating the fine spacing from the coarse spacing. The Gauss quadrature is arranged to extend over an energy region exceeding 11.2 eV. When $(T_{N-1} - T_N)$ corresponds to the first of these buffer intervals, fine spacing can resolve the peak region of the oscillator strength distribution; while for $(T_{N-1} - T_N)$ corresponding to the second of these intervals, the peak region is covered by the Gauss quadrature region, now 20 eV wide.

Coarse spacing begins with an interval of 20 eV and increases at the rate already given,

$$\Delta T_{n+1}/\Delta T_n = 2^{1/NPH} \quad . \tag{II.37}$$

Intervals increase in spacing until $T_o/2$ is exceeded, at some value T_n. For this value, one writes N2 = n, and $TY(N2) = T_o/2$. The value TY(N2 - 1) is then readjusted to give a more even sequence near $T_o/2$.

For $n > N2$, the values of $TY(n)$ repeat in reverse order those which precede, according to the rule

$$TY(n) = TY[2 \cdot N2 - n] \quad . \tag{II.38}$$

This has the consequence that the intervals decrease in width progressively towards low electron kinetic energy.

Finally, intervals may be added as necessary. In particular, 10 to 20 additional values are usually added below the lowest electronic transition energy to cover the region in which vibrational transitions are dominant. (No attempt is made in the interval near T_0 to perform corresponding calculations.)

One should note that for low source energies T_0, the sequence just described is interrupted whenever the tabulated value recorded in TY exceeds $T_0/2$. Below $T_0/2$, however, the procedure is as already outlined.

Both N2 and N3 are output constants that are recorded in memory locations available to other subroutines.

15. CXPRT(KX)

The name for this subroutine is short for "cross section printout." Output determined by this routine includes the stopping number, the total cross section and various components, including the total ionization cross section, and the function XKAP which multiplies stopping number and total cross section "number" to give stopping powers and interaction probabilities per unit path length.

For KX = 1, the differential cross section is printed as well, normalized to be compared with a Platzman plot. For KX = 0 (or negative), only the integral cross sections are recorded.

16. SOLVE(IS)

Output of this subroutine is a solution list for the index IS; the values are recorded in the array SOL(I,2-IS). Interpretation of the different possible cases is as follows:

IS = 1: The total slowing-down spectrum including secondaries of all orders;

IS = 0: primary electrons only

IS = -1: 1st generation secondaries only;

IS = -J: J'th generation secondaries only.

For IS = 1, the integration weights required are those based on inclusion of secondary electrons. For IS = 0, the integration weights are zero for secondary electron components. For negative IS values, the integration weights which are appropriate are differences between the above, i.e., weights only for secondary electrons, which are used in tandem with weights only for primary electrons.

For negative IS values, the two required sets of weights are put above and below the diagonal element of the WT array, with the diagonal reserved for WT(N,N).

The calculation proceeds by setting up an array of integration weights as called for. However, the different generations of secondary electrons are calculated in order; and all use the same array of weights, which is thus determined only once, and used for all $J \leqslant -1$.

Next, the calculation proceeds by evaluating the source contribution (ONCE), the scattering integral contribution, and finally, by use of WT(N,N), the value of y. Because the different generations of secondaries are computed in chain fashion, the solution for the preceding generation is retained in a special list, y(I), for further reference. (This is convenient rather than essential, because this information is also in the general solution array SOL.)

17. ECHEK(N,IX)

Output is the fraction of the input energy T_o which is dissipated in the form of electrons of kinetic energy lower than the N'th solution energy T, plus the energy deposited with molecules, due both to excitations and ionizations. Also computed is the number of electrons making the transition from kinetic energy above T_N to kinetic energy below T_N.

Because all energy is dissipated regardless of the criterion used, energy conservation requires a value of unity for the fraction mentioned above. Similarly, number conservation requires a value of unity for the number of electrons crossing the cut-off T_N, for T such that $T_N > (T - I)/2$ or for calculations based on the spectrum of primaries only.

The index IX merely selects the spectrum whose energy fraction is to be computed. Note that energy and number dissipation can be computed not only for the total slowing-down spectrum, but also for its various components, viz., primaries only, or n'th generation secondaries.

Let us write $\bar{k}(T',\epsilon)$ for $\frac{k(T',T)}{\kappa(T')}$ where $\epsilon = T' - T$, where κ is a function earlier called XKAP,

$$\kappa(T') = \frac{3}{4} \frac{N_A}{A} \phi_o \frac{Z}{\beta^2(T')} \quad . \tag{II.39}$$

We then define various derived quantities as follows:

$$\mathcal{K}(T',x) = \int_0^x d\epsilon\ \bar{k}(T',\epsilon), \quad \text{i.e.,} \quad TCX(T',x,IVB) \quad , \tag{II.40}$$

$$K(T') = \mathcal{K}(T',(T'+I)/2), \quad \text{also} \quad TCX(T',T',IVB) \quad , \tag{II.41}$$

$$\mathcal{S}(T',x) = \int_0^x d\epsilon\ \ \epsilon\bar{k}(T',\epsilon), \quad \text{i.e.,} \quad STN(T',x,0) \quad , \tag{II.42}$$

$$S(T') = \mathcal{S}(T',(T'+I)/2), \quad \text{also} \quad STN(T',T',0) \quad , \tag{II.43}$$

$$\mathcal{S}^*(T',x) = \mathcal{S}(T',x) + I[K(T') - \mathcal{K}(T',x)], \quad \text{i.e.,} \quad STN(T',x,1) \quad . \tag{II.44}$$

Then eq (7) is interpreted numerically with the following identifications:

$$y(T',T_0) = q_J(T',T_0)/\kappa(T') \quad , \tag{II.45}$$

$$\begin{aligned} S(T',\bar{T}) &= \kappa(T')\ \mathcal{S}^*(T',T+I), \quad T' \geq 2\bar{T} + I \quad , \\ &= \kappa(T')\ \{\mathcal{S}(T',T'-\bar{T}) + T'[K(T') - \mathcal{K}(T',T'-\bar{T})]\}, \quad T' < 2\bar{T} + I \quad . \end{aligned} \tag{II.46}$$

Similarly, eq (8) can be interpreted as follows:

$$K_p(T',\bar{T}) = \kappa(T')[K(T') - \mathcal{K}(T',T'-\bar{T})], \quad T' \leq 2\bar{T} + I \text{ and } T' < T_0 \quad , \tag{II.47}$$

$$K_S(T',\bar{T}) = \kappa(T')[K(T') - \mathcal{K}(T',\bar{T}+I)], \quad T' \geq 2\bar{T} + I \quad . \tag{II.48}$$

In both cases, solution is for $q(T',T_o)$. But to check number conservation, it is more useful to take $K_S = 0$.

The integrands of eqs. (7) and (8) become very large for $T' \approx \bar{T}$. In principle this suggests an application of Gauss quadrature. But we prefer here simply to add and subtract integral quantities with two properties: a) the modified integrands tend to vanish as $T' \to \bar{T}$; and b) the subtracted integral term can be accurately and readily evaluated. Our choice of supplementary term for evaluation of the energy conservation equation is the following identity:

$$\mathcal{I}_E = \int_{\bar{T}}^{(3\bar{T}+I)/2} dT'\ y(\bar{T},T_o)\ \bar{T}[K(\bar{T}) - \mathcal{K}(\bar{T},T'-\bar{T})] = \bar{T}\ y(\bar{T},T_o)\ S(\bar{T}) \quad . \qquad (II.49)$$

Correspondingly, we use the following term in the number conservation equation.

$$\mathcal{I}_N = \int_{\bar{T}}^{(3\bar{T}+I)/2} dT'\ y(\bar{T},T_o)\ [K(\bar{T}) - \mathcal{K}(\bar{T},T'-\bar{T})] = y(\bar{T},T_o)\ S(\bar{T}) \quad . \qquad (II.50)$$

Equations (7) and (8) then take the forms

$$\bar{T}\ y(\bar{T},T_o)\ S(\bar{T}) = T_o - \left\{ \int_{\bar{T}}^{T_o} dT'\ y(T',T_o)\ \kappa(T')\ S(T',\bar{T}) - \mathcal{I}_E \right\} \quad , \qquad (II.51)$$

$$y(\bar{T},T_o)\ S(\bar{T}) = 1 + \int_{2\bar{T}+I}^{T_o} dT'\ y(T',T_o)\ \kappa(T')\ K_S(T',\bar{T})$$

$$- \left\{ \int_{\bar{T}}^{2\bar{T}+I} dT'\ y(T',T_o)\ \kappa(T')\ K_P(T',\bar{T}) - \mathcal{I}_N \right\} . \qquad (II.52)$$

If one combines terms in braces into single integrals, one finds that the integrands then approach zero in the limit of $T' \to T$. One remaining question pertains to whether the approach to zero may not be so slow that the contribution of the final interval is, say, underestimated; this can in principle be a significant problem because of an often sizable contribution due to this interval. To keep track of this, an extrapolation of the integrand to a finite value, rather than zero, has been made, with an associated estimate of the corresponding modification to the integrated result. On the basis of this estimate, the problem did not appear to be serious.

The above addition-subtraction is <u>not</u> carried out below the lowest electronic transition energy, taken to be THR = 11.25 eV. In that low energy region, evaluation of the integrands is carried out directly.

The outline of the computation is as follows: First, a list of integration weights is computed, using the Stieltjes integration method described in section II.11. This method was not essential; but the intervals vary in size, and this is a suitable way to take account of these variations. Next, the numerical integration sum is evaluated; and evaluations of the addition-subtraction and the source term follow. These three terms, their sum, and the extrapolation fractional increment used to check the addition-subtraction procedure are recorded for possible output. A sixth quantity is also evaluated, namely the number of electrons crossing the specified energy cut-off T_N.

In addition, three other quantities are routinely evaluated. One of these is the value of $1/W(T)$, number of ions per eV generated by $y(T')$, $T' > T$. The second is the total yield of excitations. The third is the factor by which the solution $y(T_N,T_o)$ must be modified to bring about accurate energy conservation. These last three quantities are stored separately from the other 6 quantities.

18. ELSPEL

Output of ELSPEL constitute the main results of the computation, including stopping powers and cross sections, the value for W, the yield of excitations of all types, the slowing-down spectrum and its components, and the results of the energy-and number-conservation tests.

Input quantities are as follows:

NEX: the number of source energies,

IX: the number of solution lists. IX = 1 here corresponds to the slowing-down spectrum alone. IX = 2 calls for a calculation also of the primaries as a separate component. IX = 3 calls for the 1st-generation secondaries as well, etc.

SORS(I): the list of source energies, in eV.

BCOR(I): see BMOD

NO, N1: see TLIST.

B: the value of b_∞.

In addition, NPH determines the number of solution energies and their separation, as discussed in TLIST.

The main DO-loop permits the computations to be repeated for different NPH values (see also TLIST), to check effects due to size of integration mesh. In this DO-loop the solution energies are first fixed, by calling TLIST. Then CXPRT is called to record various stopping powers and cross sections. Next HARDP performs the preliminary computations of necessary energy-dependent parameters. SOLVE is then called to compute the slowing-down spectrum; and this computation is followed by print-out of results,

together with related quantities including the integrand for computation of (1/W). Finally, ECHEK performs the energy- and number-conservation tests, and values for W and any for excitation yields.

The whole computation can then be repeated at other value of T_o, if NEX > 1, or possibly with a different set of integration points.

Other special cross section routines are sometimes inserted in ELSPEL.

Table Captions

Table 1 Integration energies for a calculation with T_o = 1 keV.

Table 2 Values for energy and number conservation integrals above different T, expressed as fractions of the source energy T_o, for T_o = 30 keV. For the column on the far right, integration was carried out only over the primary component.

Table 3 Ratios $y(T,T_o)/y(T,1\ MeV)$, for various T,T_o.

Table 4 Experimental and theoretical values for W, FE, F, and DS refer to Fowler equation, (Fano) energy balance, and degradation spectrum methods of calculation [55].

Table 5 Volts per ion pair (W) as computed for different source electron kinetic energies.

Table 6 Some comparisons with data from reference [15].

Table 1. Integration energies for a calculation with T_o = 1 keV.

n	(T_o-T),eV	n	(T_o-T),eV	n	T,eV	n	T,eV	n	T,eV
1	11.43	28	31.74	55	404.4	82	29.42	109	10.43
2	11.87	29	32.96	56	308.7	83	28.33	110	9.93
3	12.33	30	34.23	57	212.8	84	27.28	111	9.43
4	12.80	31	35.55	58	145.2	85	26.27	112	8.93
5	13.29	32	36.92	59	102.7	86	25.29	113	8.43
6	13.81	33	38.34	60	82.7	87	24.35	114	7.93
7	14.34	34	39.82	61	72.7	88	23.45	115	7.43
8	14.89	35	41.36	62	62.7	89	22.58	116	6.93
9	15.47	36	42.95	63	60.37	90	21.74	117	6.43
10	16.06	37	44.61	64	58.13	91	20.93	118	5.93
11	16.68	38	46.33	65	55.97	92	20.16	119	5.43
12	17.33	39	48.11	66	53.90	93	19.41	120	4.93
13	17.99	40	49.97	67	51.90	94	18.69	121	4.43
14	18.69	41	51.90	68	49.97	95	17.99	122	3.93
15	19.41	42	53.90	69	48.11	96	17.33	123	3.43
16	20.16	43	55.97	70	46.33	97	16.68	124	2.93
17	20.93	44	58.13	71	44.61	98	16.06	125	2.43
18	21.74	45	60.37	72	42.95	99	15.47	126	1.93
19	22.58	46	62.70	73	41.36	100	14.89	127	1.43
20	23.45	47	72.70	74	39.82	101	14.34		
21	24.35	48	82.70	75	38.34	102	13.81		
22	25.29	49	102.7	76	36.92	103	13.29		
23	26.27	50	145.2	77	35.55	104	12.80		
24	27.28	51	212.8	78	34.23	105	12.33		
25	28.33	52	308.7	79	32.96	106	11.87		
26	29.42	53	404.4	80	31.74	107	11.43		
27	30.56	54	500	81	30.56	108	10.93		

Table 2. Values of energy and number conservation integrals between T_o and T, expressed as fractions of T_o, for T_o = 300 keV

For the column on the far right, integration was carried out only over the primary component.

T_o-T,eV	Energy Conservation	Number Conservation	T,eV	Energy Conservation	Number Conservation
16.1	.981	.981	8925	.981	.993
23.4	.982	.982	3843	.988	.992
34.2	.986	.986	1350	.994	.993
50.0	.992	.992	308.7	1.007	1.004
145.2	1.000	1.000	72.7	1.012	.972
803.	.992	.997	44.6	1.016	.979
2,614	.989	.993	30.6	1.015	.971
13,546	.981	.992	20.9	1.013	.971
			14.3	1.022	.991
			9.43	1.029	.981
			4.43	1.028	1.005
			1.93	1.012	.833

Table 3. Ratios $y(T,T_o)/y(T,1\ MeV)$, for various T,T_o.

T_o, keV	T = 9.9	12.3	17.3	22.6
.10	1.376	1.470	1.813	2.197
.30	1.132	1.163	1.279	1.401
.50	1.112	1.134	1.211	1.288
1.0	1.0775	1.0922	1.144	1.190
3.0	1.0564	1.0653	1.0965	1.122
5.0	1.0490	1.0564	1.0824	1.103
10.	1.0394	1.0453	1.0658	1.0822
30.	1.0269	1.0308	1.0448	1.0558
100	1.0159	1.0181	1.0265	1.0304
300	1.0080	1.0090	1.0133	1.0166

Table 4. Experimental and theoretical values for W (see also Whyte [56] and Booz and Ebert [21]). FE, F, and DS refer to Fowler equation, (Fano) energy balance, and degradation spectrum methods of calculation [55].

Experiments with Electrons	Experiments with Heavy Particles	Calculations (1 keV)
36.3 (^{3}H β rays) [35]	36.3 (Po α rays) [35,43]	37.12 [51], FE
35.9 (^{3}H β rays) [36,35]	37.0 ± .4 (Pu α rays) [44]	40.12 [3], FE
36.3 ± .7 (2 MeV x-rays) [37]	36.0 ± .15 (Po α rays) [45]	38.63 [24], FE
37.0 ± .3 (^{60}Co γ rays) [38]	36.2 (340 MeV protons) [46]*	35.0 [52], F
37.0 (.4 - 1 keV β rays) [39]	36.01 (Pu α rays) [47]	36.3 [2], DS, FE
37.8 (2 MeV electrons) [40]	36.1 (Po α rays) [48]	35.9 [53], FE
37.2 (^{37}A β rays) [41]	35.3 (Po α rays) [49,83]	35.3 [54], FE
38.0 (^{3}H β rays) [41]	37.0 (Po α rays) [50]	
38.0 (^{3}H β rays) [42]*		

*Based on W = 26.2 for Ar.

Table 5. Volts per ion pair (W) as computed for different source electron kinetic energies

T, keV	W
.024	69.4
.027	73.2
.030	67.4
.035	56.5
.05	50.7
.07	47.1
.1	44.2
.3	39.27
.5	37.44
1.	36.24
2.	36.03
3.	36.05
5.	36.08
10.	36.20
30.	36.40
100.	36.59
300.	36.75
1000.	36.90

Table 6. Some comparisons with data from reference [1].

T(eV)	y (cm/eV)	Okazaki-Sato
10^4	$.26 \times 10^{-3}$	$.46 \times 10^{-3}$
10^3	$.23 \times 10^{-3}$	$.43 \times 10^{-3}$
10^2	$.80 \times 10^{-3}$	1.22×10^{-3}

Table Captions - Appendix I

Table I.1 Oscillator strengths for discrete excitations [3], based on Allison and Dalgarno [59] and Namioka [29].

Table I.2 Tabulations of moments of the OSD, as defined in eqs (II.1) and (II.2).

Table I.3 A tabulation of low energy correction functions for ionization ($\ell n\ b_\infty/b$) using $b_\infty = 3$, and excitation ($\ell n\ 1/b_1$).

Table I.4 Comparisons of total ionization and excitation cross sections for electrons with kinetic energies below 1000 eV. See references [3,33]. (The number of digits given is for comparisons; neither type of cross section is known to any such accuracy.)

Table I.5 Vibrational cross sections for the two lowest excitations, used in conjunction with eqs (8) and (9) and due to Trajmar, et al [64].

Table I.6 Values of $\langle I \rangle$, the mean excitation potential for molecular hydrogen.

Table Captions - Appendix II

Table II.1 Description of ELSPEL subprograms. Abbreviations are as follows: c.s.--cross section, c.c.s.--combined cross section, sc.int--scattering integral, eval.--evaluation

Table I.1 Oscillator Strengths for discrete excitations [3], based on Allison and Dalgarno [59], and Namioka [29].

E_n, eV	Lyman f_n	E_n, eV	Werner f_n
11.213	.001709	12.317	.05246
11.377	.005859	12.605	.08027
11.535	.01170	12.875	.07694
11.674	.01776	13.129	.06030
11.846	.02277	13.367	.04269
11.982	.02602	13.589	.02863
12.132	.02736	13.794	.01873
12.268	.02705	13.984	.01211
12.405	.02553	14.156	.007822
12.524	.02326	14.319	.005060
12.679	.02059	14.446	.003280
12.790	.01785	14.560	.002104
12.902	.01522	14.650	.001290
13.026	.01281	14.710	.000616
13.139	.01068		
13.238	.008835		
13.305	.007271		
13.450	.005962		
13.549	.004878		
13.648	.003986		
13.735	.003258		
13.822	.002664		
13.909	.002180		
13.996	.001787		
14.071	.001467		
14.150	.001207		
14.220	.0009933		
Total	.3107	Total	.3923

Table I.2. Tabulations of moments of the OSD, as defined in eqs. (II.1) and (II.2).

Excitations

Energy	I =	$\mathcal{S}_m^e$			$\mathcal{L}_m^e$		
		1	2	3	1	2	3
11.2130		.0000	.0000	.0000	.0000	.0000	.0000
11.6450		.0229	.0193	.0162	.0080	.0068	.0057
12.0940		.0992	.0858	.0742	.0350	.0302	.0262
12.5610		.2710	.2415	.2153	.1011	.0902	.0805
13.0450		.5095	.4652	.4258	.2015	.1843	.1689
13.5480		.6489	.6008	.5580	.2608	.2420	.2252
14.0700		.7260	.6791	.6370	.2937	.2754	.2589
14.6130		.7782	.7361	.6975	.2912	.2748	.2582
15.1760		.8506	.8153	.7841	.2738	.2542	.2356
15.7610		.9052	.8771	.8543	.2586	.2370	.2161
16.3690		.9231	.8982	.8791	.2536	.2312	.2092
17.0000		.9283	.9045	.8868	.2522	.2294	.2071

Ionizations

	$\mathcal{S}_m^i$			$\mathcal{L}_m^i$		
15.1760	.0000	.0000	.0000	.0000	.0000	.0000
15.7610	.0113	.0130	.0148	.0309	.0357	.0410
16.3690	.0548	.0644	.0758	.1415	.1787	.2102
17.0000	.1069	.1283	.1542	.2984	.3585	.4307

Table I.3. A tabulation of low energy correction functions for ionization ($\ell n\ b_\infty/b$) using $b_\infty = 3$, and excitation ($\ell n\ 1/b_1$).

T, eV	$\ell n\ (b_\infty/b)$	$\ell n\ (1/b_1)$
1414	.00	.000
1000	.13	.000
707	.25	.000
500	.40	.000
353.6	.62	.000
250	.90	.010
176.8	1.23	.175
125	1.54	.408
88.4	1.78	.614
62.5	1.93	.819
44.2	1.99	1.037
31.25	2.02	1.185
22.1	1.92	1.210
18.58	1.79	
15.625	2.40	1.100
14.00		.98
11.05	3.20	.81

Table I.4. Comparisons of total ionization and excitation cross sections for electrons with kinetic energies below 1000 eV. See refs. [3,33]. (The number of digits given is for comparisons; neither type of cross section is known to any such accuracy.)

	σ_{ion}, πa_o^2 units			$\sigma_{exc} \times 10^{17}$ cm^2	
T	Rapp-Englander-Golden	This Effort	T, eV	Gerhart	This Effort
1000	.273	.265	360	5.41	5.43
500	.462	.461	320	5.96	5.95
300	.651	.650	240	7.34	7.24
250	.723	.725	160	9.27	9.25
150	.924	.923	120	10.61	10.54
140	.944	.947	100	11.40	11.38
125	.982	.983	80	12.23	12.24
100	1.05	1.048	70	12.67	12.66
85	1.089	1.081	60	13.06	12.95
70	1.104	1.103	50	13.19	12.90
60	1.10	1.102	40	12.69	12.32
50	1.07	1.078	30	10.64	10.59
40	.984	.987	20	7.08	7.18
34	.882	.874	15	2.35	2.42
24	.550	.538	11.2	0	0
19	.250	.258			
18	.177	.161			
16.5	.069	.073			

Table I.5. Vibrational cross sections for the two lowest excitations, used in conjunction wih eqs. (8) and (9) and due to Trajmar, et al [64].

	$\frac{T\sigma}{4\pi a_o^2 R}$	
T, eV	0.54 eV	1.08 eV
1.3	0	0
1.6	.0081	.000110
2.0	.0162	.000560
2.5	.0251	.00147
3.0	.0321	.00220
3.5	.0374	.00276
4.0	.0389	.00324
5.0	.0383	.00360
6.0	.0357	.00382
7.0	.0329	.00391
8.0	.0254	.00391
9.0	.0229	.00320
10.0	.0181	.00205
14.0	.00819	.000737
20.0	.00585	.000199

Table I.6 Values of $\langle I \rangle$, the mean excitation potential for molecular hydrogen.

Experiments		Calculations		Summary Estimates	
17.1 ± .3	[66]	19.5 ± .5	[74]	18.2	[79]
18.3 ± 2.6	[67,68,69]	18.6	[75]		
20.4 ± .9*	[70]	18.7 ± .2	[76]	18.8 ± .5	[80]
18.9	[46,71]	19.21	[77]	18.0	[81]
21.6	[72,73]	19.2	[3]		
		19.26	[78,73]	19.2	[82]
		19.22 (B)	Our values		
		18.6 (P)			

*Liquid hydrogen

Table II.1. Description of ELSPEL subprograms. Abbreviations are as follows: c.s.--cross section, c.c.s.--combined cross section, sc.int.--scattering integral, eval.--evaluation

SUBPROGRAM	TYPE	DEPENDENCE	PURPOSE OR CONTEXT
OSCUM	c.s.		cumulative oscillator strength
VIB	c.s.		vibrational cross sections
BMOD	c.s.		low energy glancing c.s. parameters
DTU	c.s.	BMOD	glancing c.s. limits
TCX	c.c.s.	all c.s.	cumulative cross sections
TCXI	c.c.s.	all c.s.	cumulative ioniz. c.s.
STN	c.c.s.	all c.s.	cumulative stopping power
ONCE	c.c.s.	all c.s.	differential cross sections
HARDP	sc.int.	DTU	factors, parameters for integration
CUMK2	sc.int.	all c.s., HARDP,TCX	Gauss quadrature, final interval
CUMK3	sc.int.	all c.s.	cumulative integrations
CORRX	sc.int.		correction for cut-off discontinuity
WATES	sc.int.	all other sc.int.	array of integration weights
TLIST	eval.		prepare list of solution energies
ECHEK	eval.	all c.c.s.	evaluate energy, number conservation
SOLVE	eval.	WATES,ONCE, ECHEK	evaluate slowing-down spectrum
CXPRT	eval.	all c.c.s.	evaluate total c.s., stopping powers
ELSPEL	master	all eval.	direct all computations, output

Figure Captions

Fig. 1 Differential cross sections for electrons of kinetic energy T_o as a function of energy loss, $T_o - T$. Secondary electrons comprise that part of the spectra below $(T_o - 16)/2$ eV.

Fig. 2 Differential cross sections for secondary electrons of final energy E due to 500 eV and 100 eV electrons in H_2. Solid curves are calculated from our cross section representations (R = 13.6 eV). The 500 eV curve agrees closely with Gerhart's data from his Fig. 7, for $E^{-1} \gtrsim .05$. Circles are Opal, Beaty, and Peterson data [30] divided by 1.65. The + values are unpublished data due to Dubois and Rudd [31].

Fig. 3 The stopping power for H_2. The dashed line gives results for the Bethe stopping power formula using 19.22 eV for the mean excitation potential. The circles give recent data due to Green [32].

Fig. 4 Total cross section for inelastic interactions of fast electrons in H_2. Also given is the fraction due to ionizing interactions.

Fig. 5 Relative contributions to the energy dissipated to kinetic energies below 16 eV, as a function of the kinetic energy of the source electrons.

Fig. 6 The Lewis effect for a 1 MeV source. S(T) is the stopping power. Solution intervals in the Lewis effect region varied from ~ 0.4 eV at $(T_o - T) \sim 11$ eV, to ~ 2 eV at $(T_o - T) \sim 60$ eV. The solution was modified to improve energy conservation in the region between the arrows at the bottom.

Fig. 7 Suitably scaled electron slowing-down spectra for source energies of 30 eV, 300 eV, 3 keV, and 30 keV. S(T) is the stopping power. For the 30 keV source, primaries and 1st generation secondaries are indicated with dashed lines. The ratio k_1/S is also given (heavy dashed line), as are several relevant reciprocal stopping numbers (at the right). Below about 12 eV, data for the three higher source energies are so close together that they are all represented by a single curve.

Fig. 8 Volts per ion pair (W) as a function of electron kinetic energy in H_2. Comparison points are given for Combecher's experimental values [57], and calculated values from references [2] and [3].

Fig. 9 Volts per ion pair (W) in H_2, for electron kinetic energies greater than 1 keV. The scale is enlarged so that small differences of trend can be readily seen. At the right, a change of 1% is exhibited. The circles give values due to Garvey, Porter and Green [2], as read from their curve. Green, Jackman, and Garvey (see [2]) give a few numerical values which are in agreement to three significant figures.

Fig. 10 Comparison of values for G = 100/W. The solid line represents our calculations. Circles give Combecher's experimental data [57]. Recent calculations due to Douthat are also shown [54].

Fig. 11 The slowing-down spectrum of 10 keV electrons in H_2, compared with values due to Douthat [1,54] and due to Garvey, Porter, and Green [2].

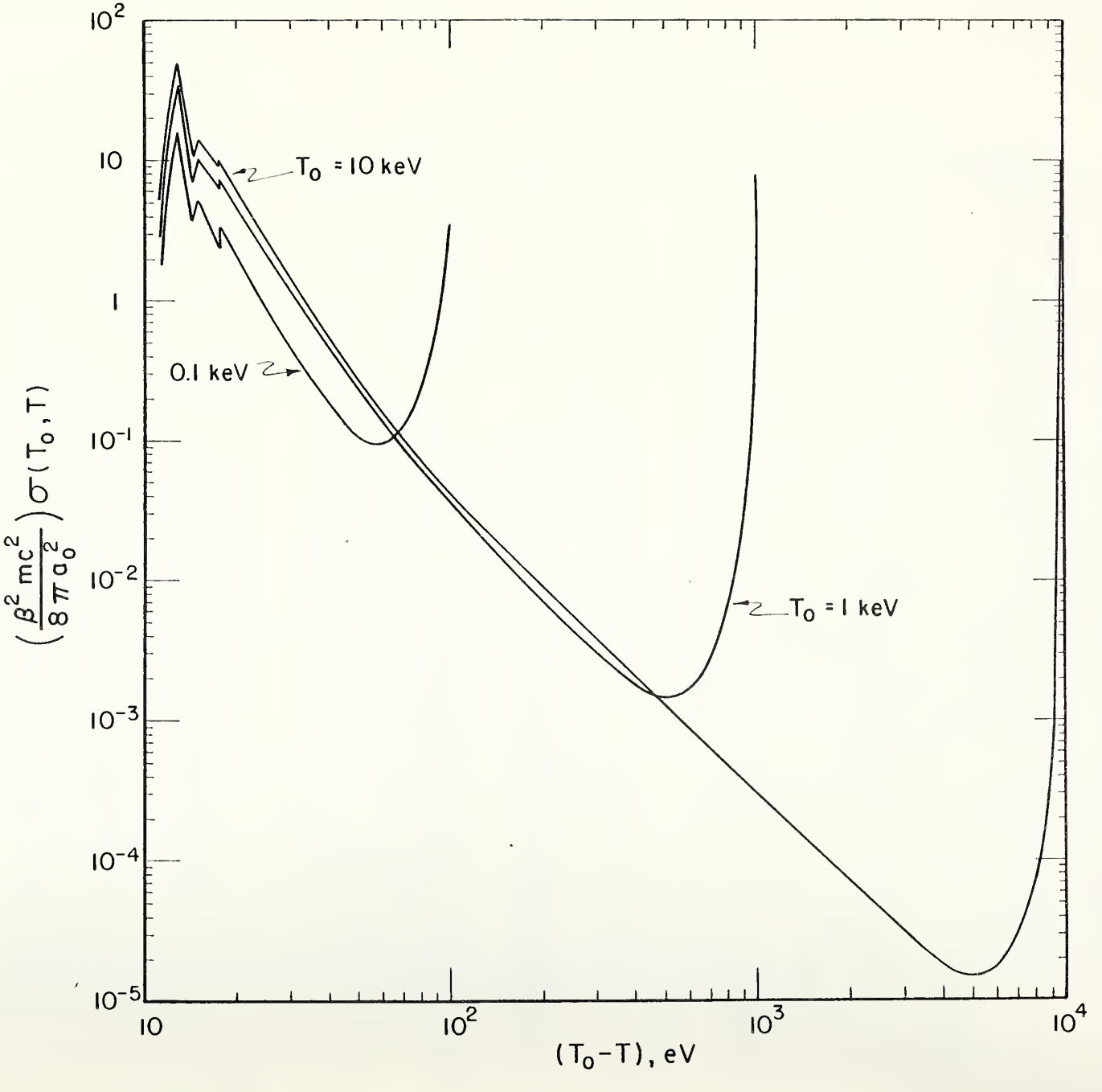

Fig. 1 Differential cross sections for electrons of kinetic energy T_o as a function of energy loss, $T_o - T$. Secondary electrons comprise that part of the spectra below $(T_o - 16)/2$ eV.

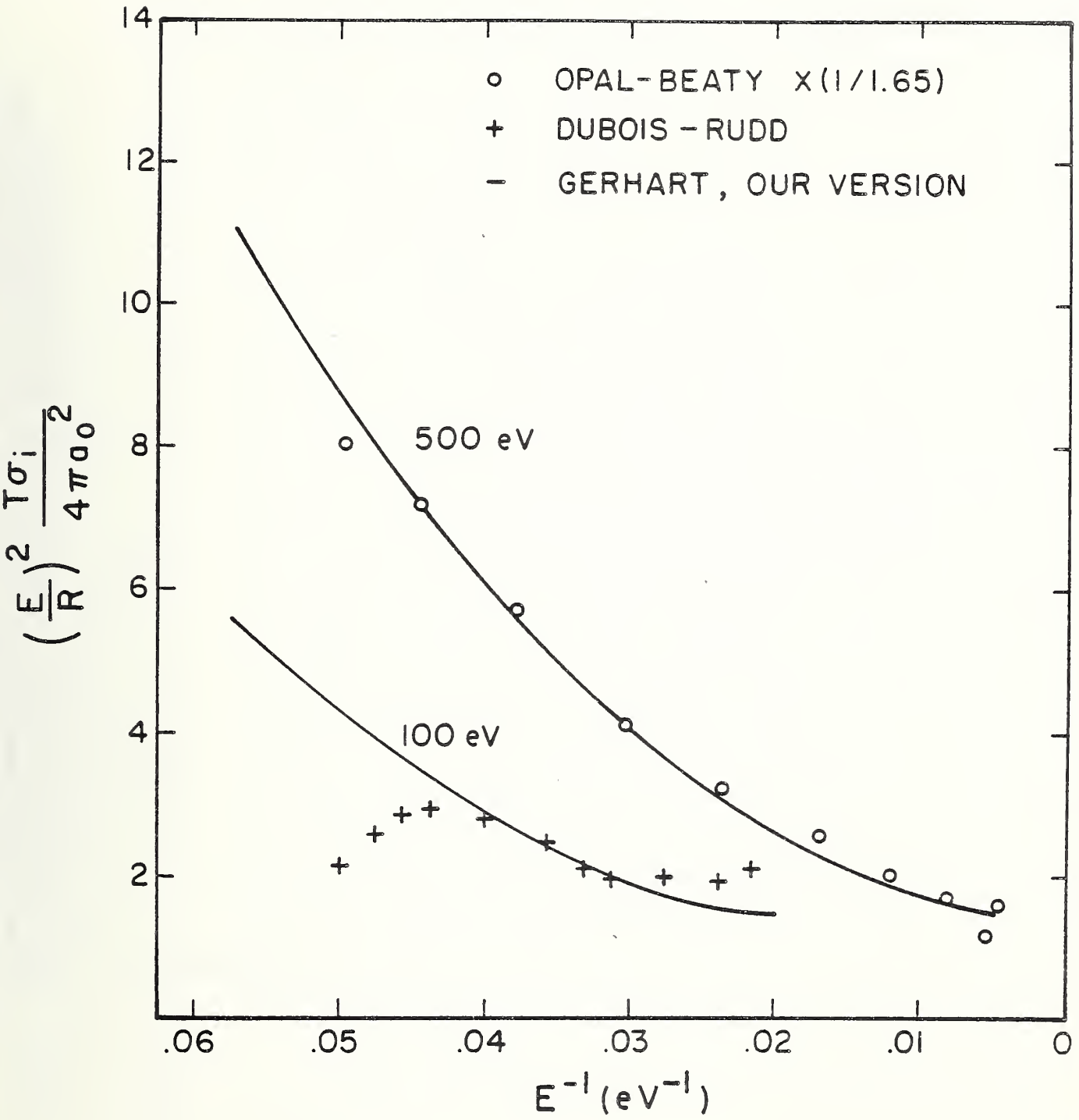

Fig. 2 Differential cross sections for secondary electrons of final energy E due to 500 eV and 100 eV electrons in H_2. Solid curves are calculated from our cross section representations (R = 13.6 eV). The 500 eV curve agrees closely with Gerhart's data from his Fig. 7, for $E^{-1} \gtrsim .05$. Circles are Opal, Beaty, and Peterson data [30] divided by 1.65. The + values are unpublished data due to Dubois and Rudd [31].

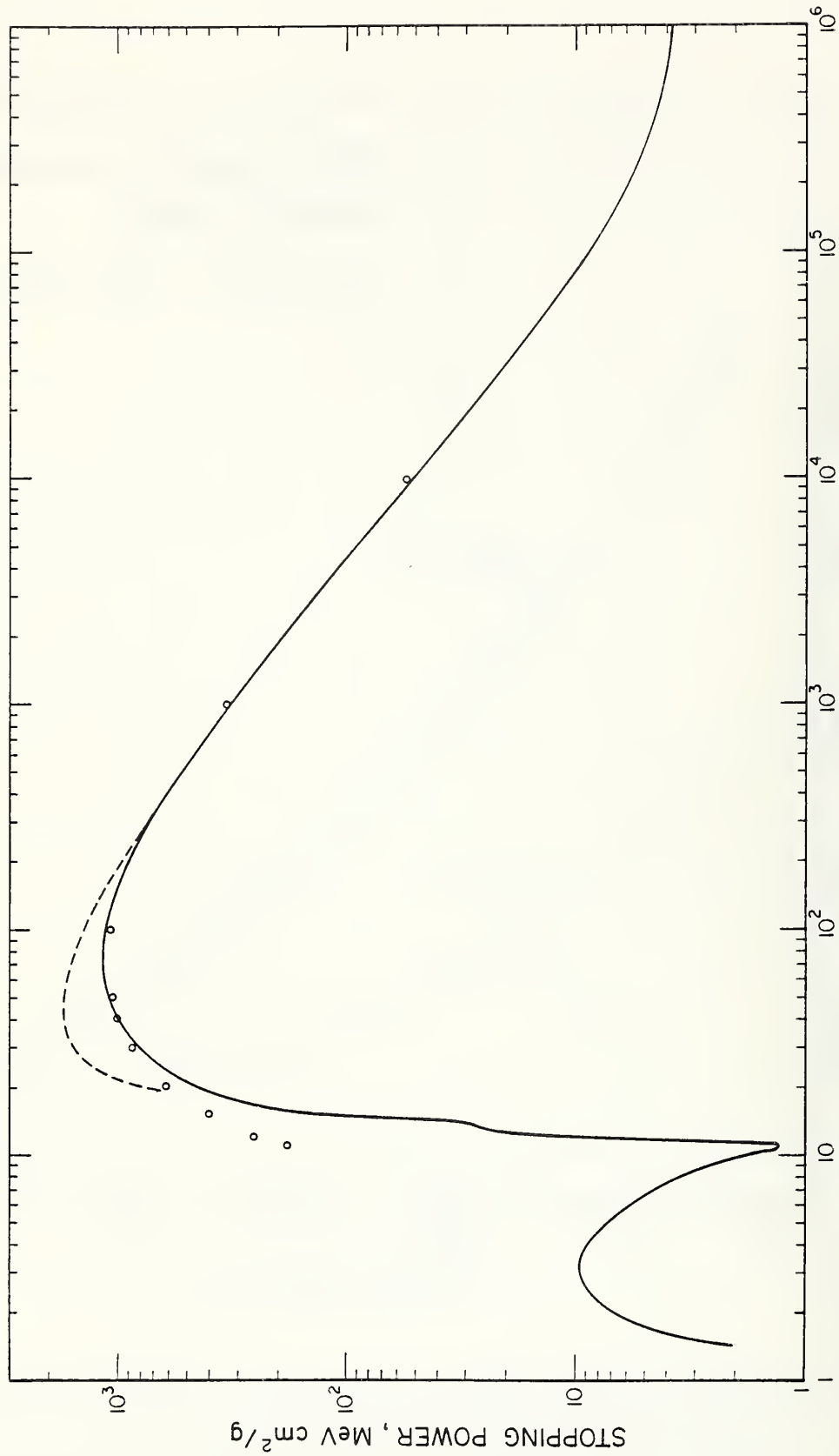

Fig. 3 The stopping power for H_2. The dashed line gives results for the Bethe stopping power formula using 19.22 eV for the mean excitation potential. The circles give recent data due to Green [32].

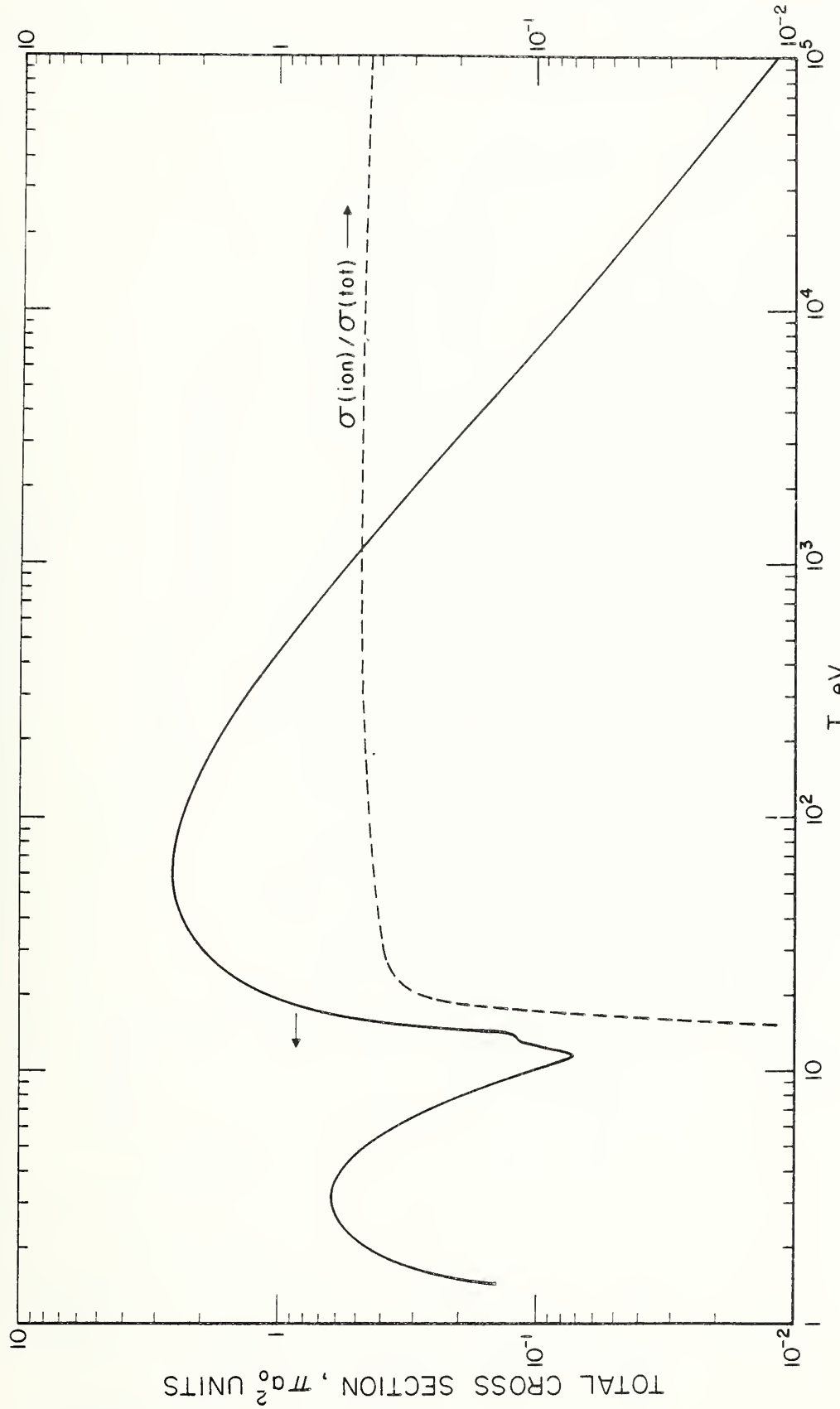

Fig. 4 Total cross section for inelastic interactions of fast electrons in H_2. Also given is the fraction due to ionizing interactions.

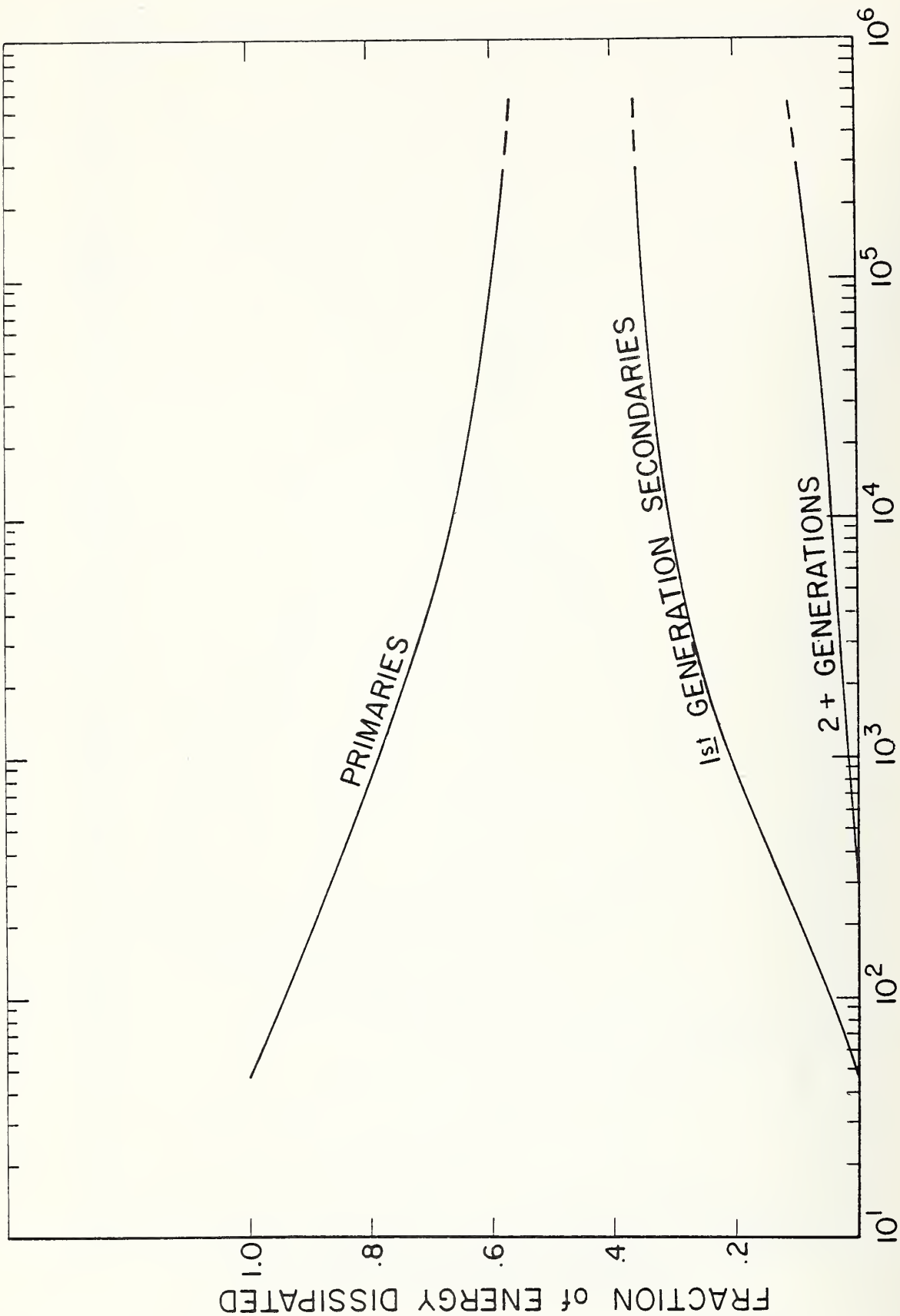

Fig. 5 Relative contributions to the energy dissipated to kinetic energies below 16 eV, as a function of the kinetic energy of the source electrons.

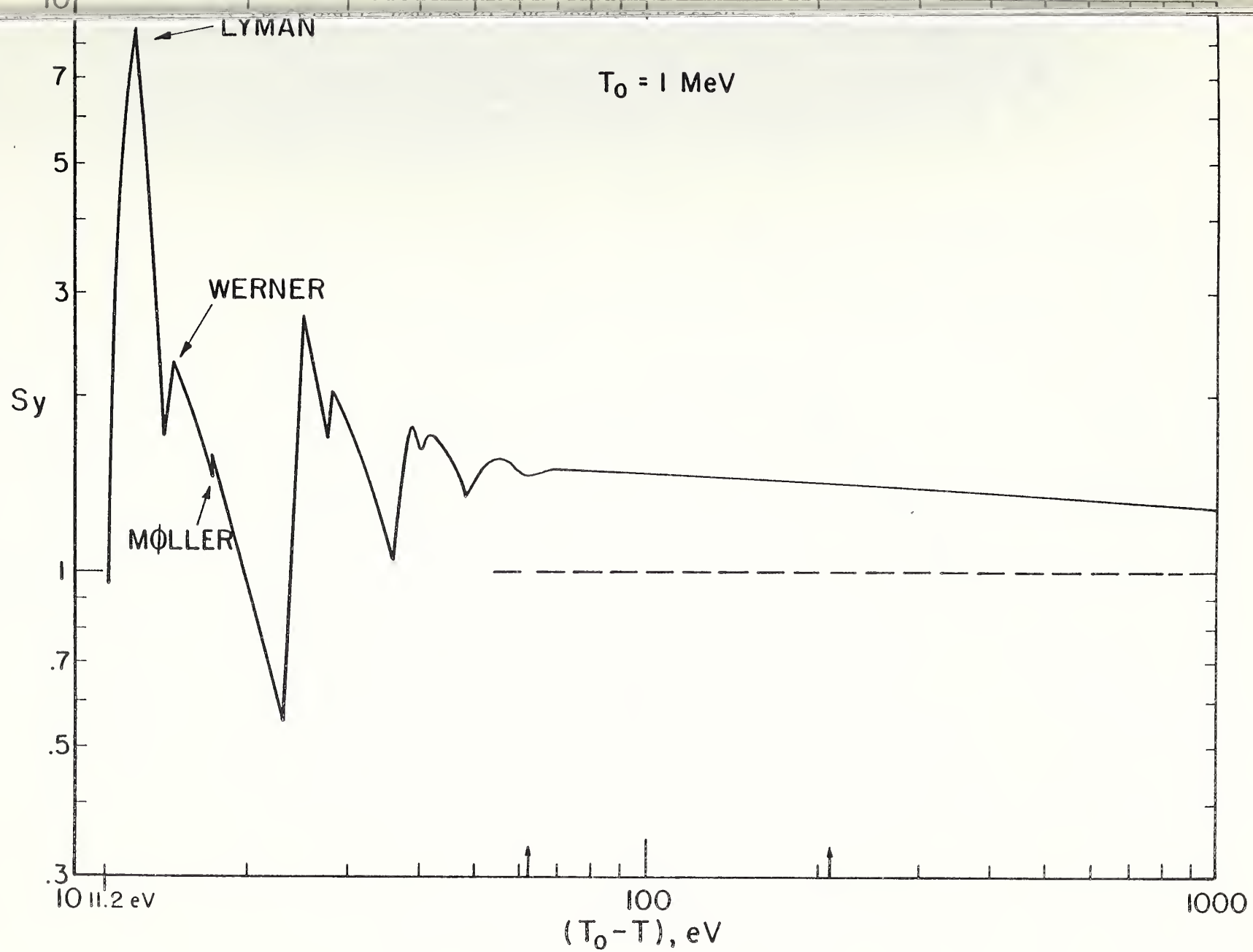

Fig. 6 The Lewis effect for a 1 MeV source. S(T) is the stopping power. Solution intervals in the Lewis effect region varied from ~ 0.4 eV at (T_0-T) 11 eV, to ~ 2 eV at (T_0-T) ~ 60 eV. The solution was modified to improve energy conservation in the region between the arrows at the bottom.

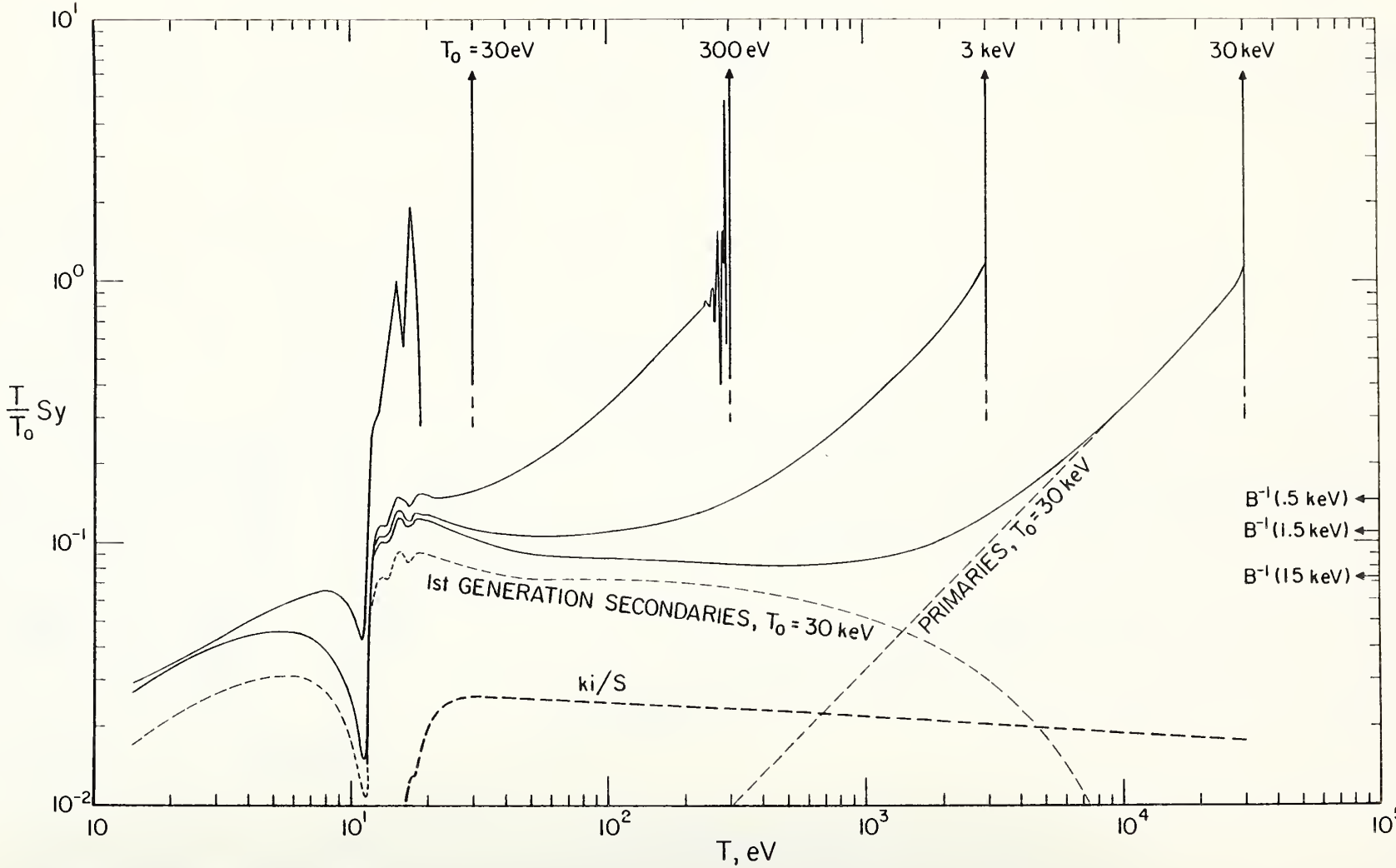

Fig. 7 Suitably scaled electron slowing-down spectra for source energies of 30 eV, 300 eV, 3 keV, and 30 keV. S(T) is the stopping power. For the 30 keV source, primaries and 1st generation secondaries are indicated with dashed lines. The ratio k_i/S is also given (heavy dashed line), as are several relevant reciprocal stopping numbers[1] (at the right). Below about 12 eV, data for the three higher source energies are so close together that they are all represented by a single curve.

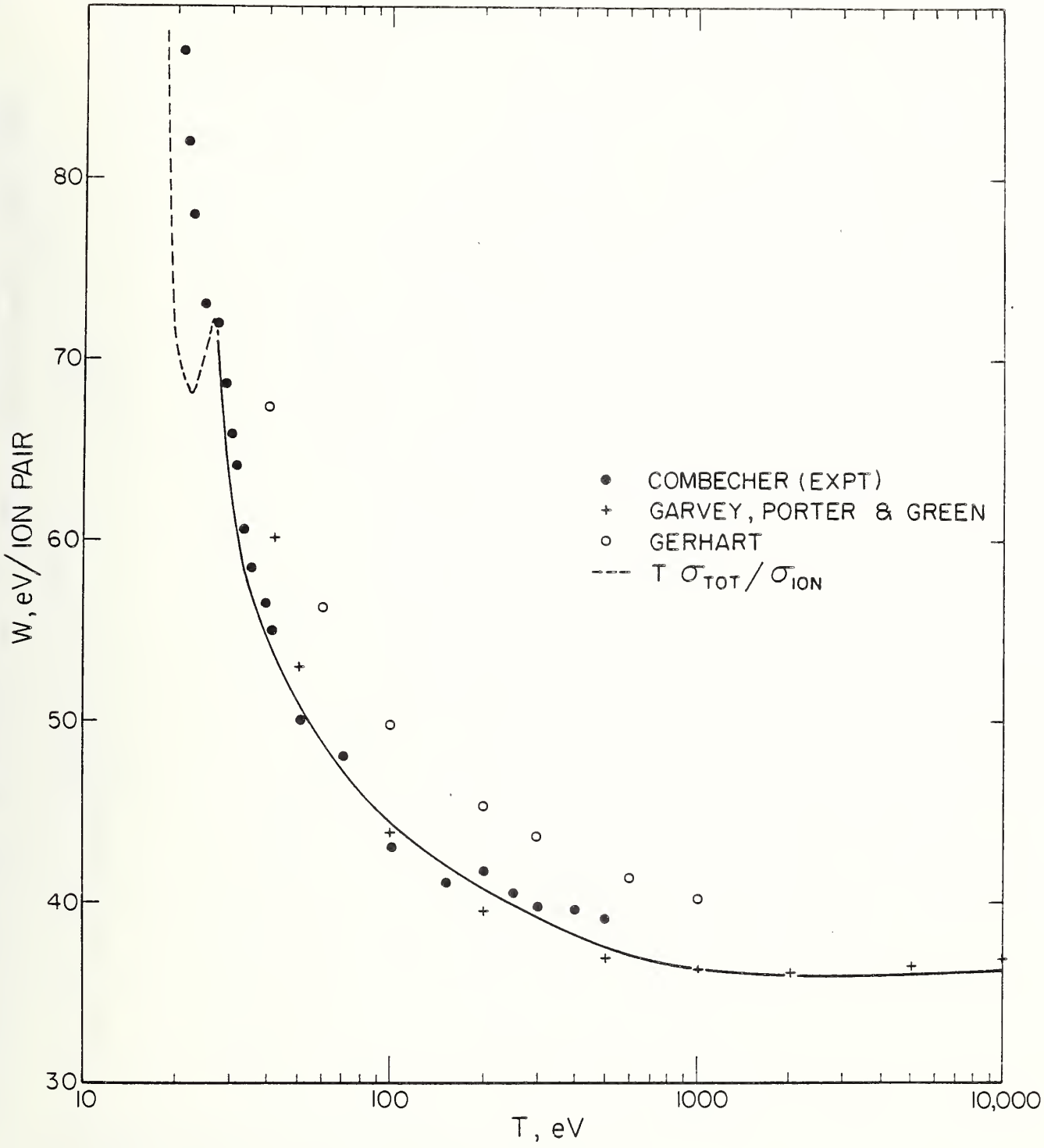

Fig. 8 Volts per ion pair (W) as a function of electron kinetic energy in H_2. Comparison points are given for Combecher's experimental values [57], and calculated values from references [2] and [3].

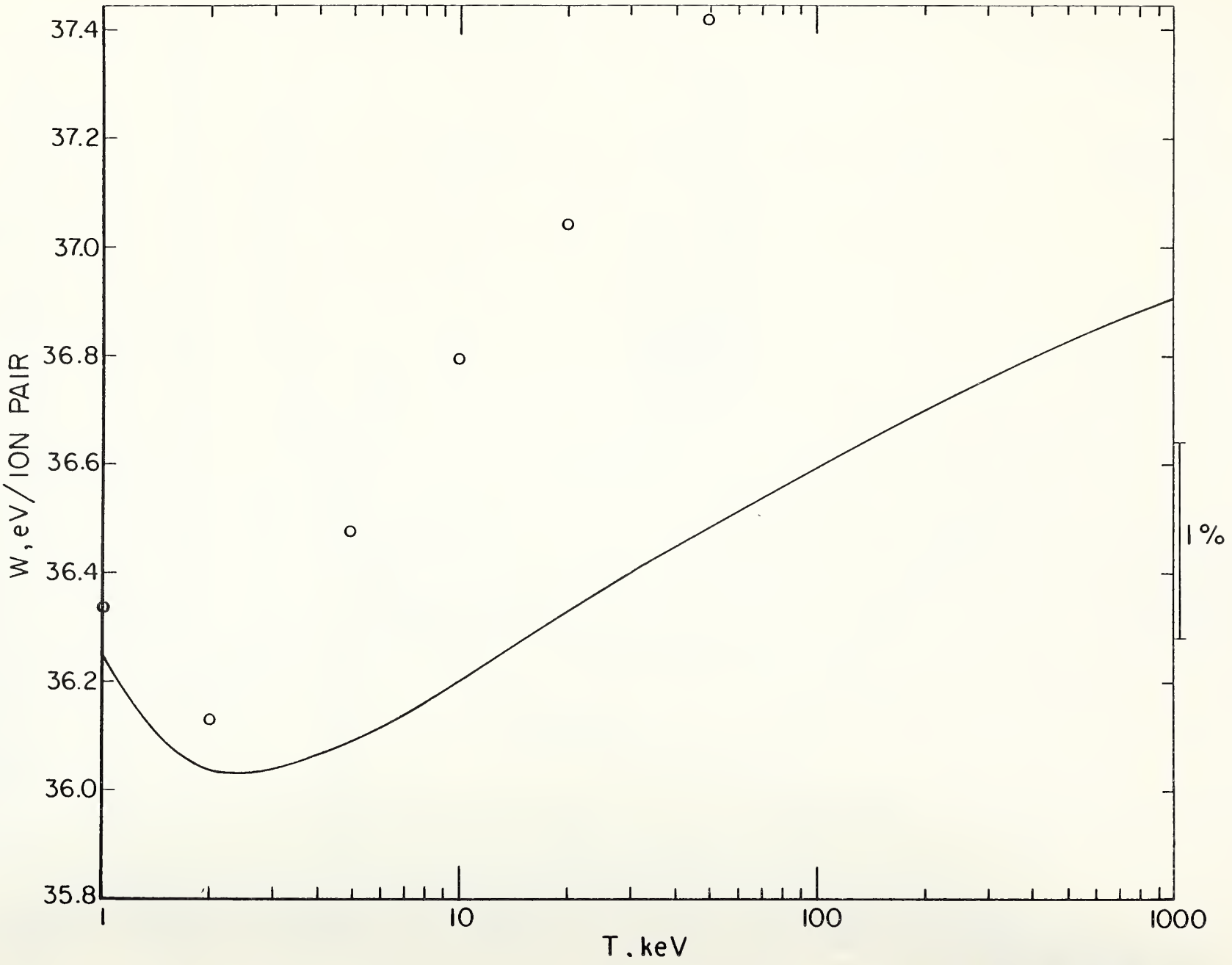

Fig. 9 Volts per ion pair (W) in H_2, for electron kinetic energies greater than 1 keV. The scale is enlarged so that small differences of trend can be readily seen. At the right, a change of 1% is exhibited. The circles give values due to Garvey, Porter and Green [2], as read from their curve. Green, Jackman, and Garvey (see [2]) give a few numerical values which

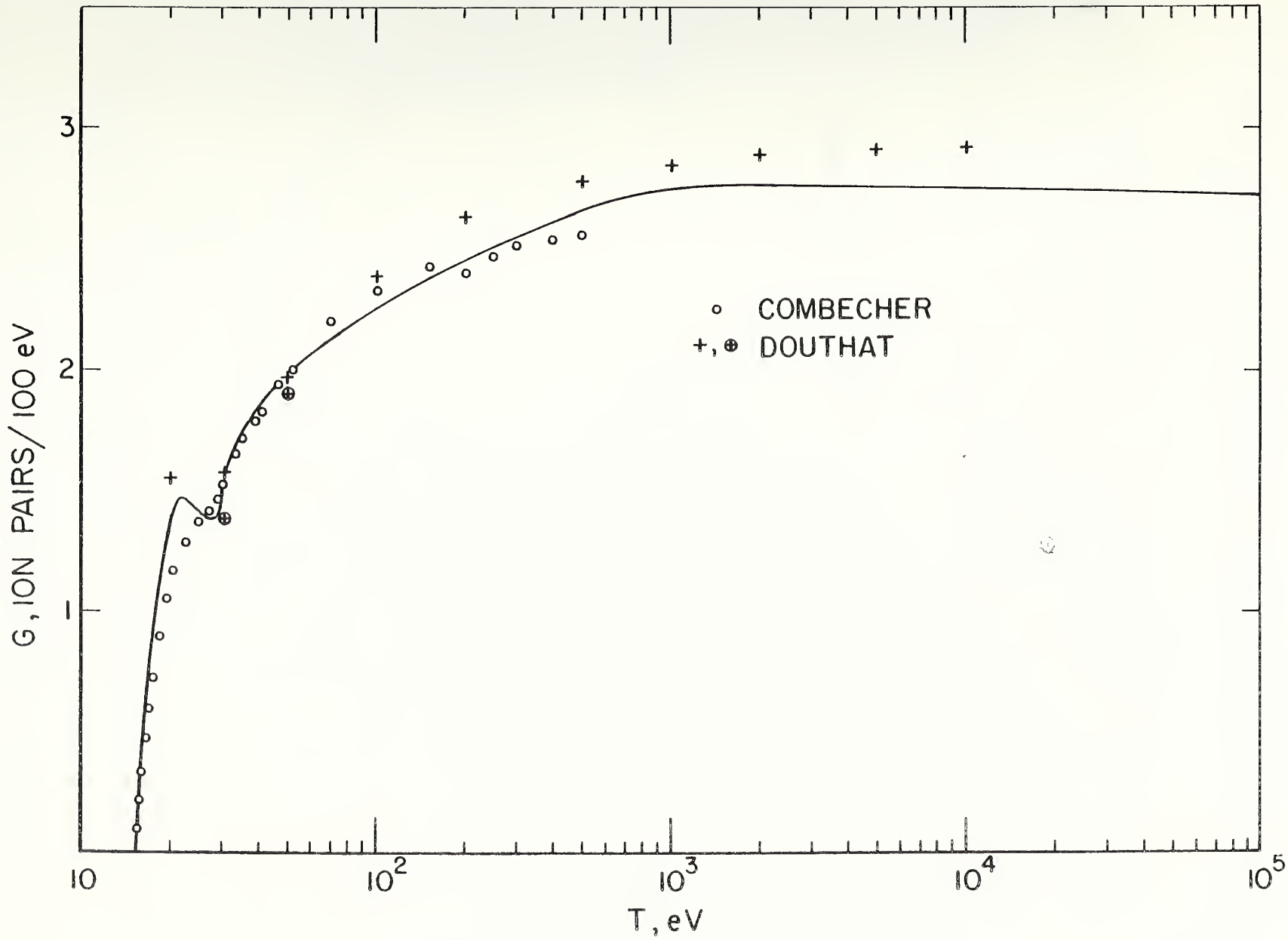

Fig. 10 Comparison of values for G = 100/W. The solid line represents our calculations. Circles give Combecher's experimental data [57]. Recent calculations due to Douthat are also shown [54].

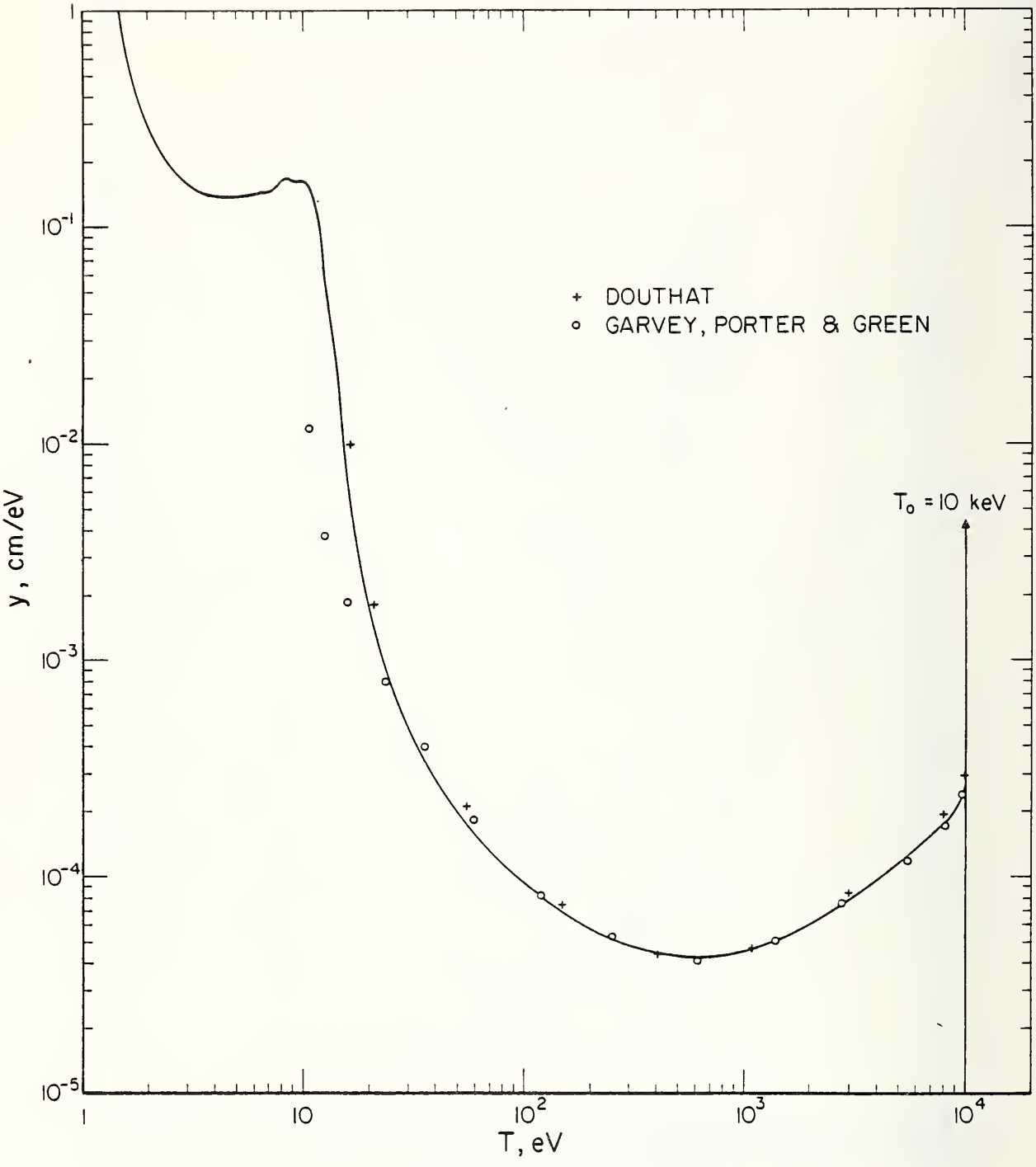

Fig. 11 The slowing-down spectrum of 10 keV electrons in H_2, compared with values due to Douthat [1,54] and due to Garvey, Porter, and Green [2].

Figure Captions - Appendix I

Fig. I.1 The ionization efficiency function as reproduced from [3]. The solid curve is due to Berkowitz [61]. The dashed line is a smoothed form due to Gerhart. The dash-dot line is due to eq (I.3).

Fig. I.2 Gerhart's $\Phi(E)$ (heavy curve) is reproduced from his Fig. 6 [3]. The light curve expresses a unit function with cut-off at 17.5 eV.

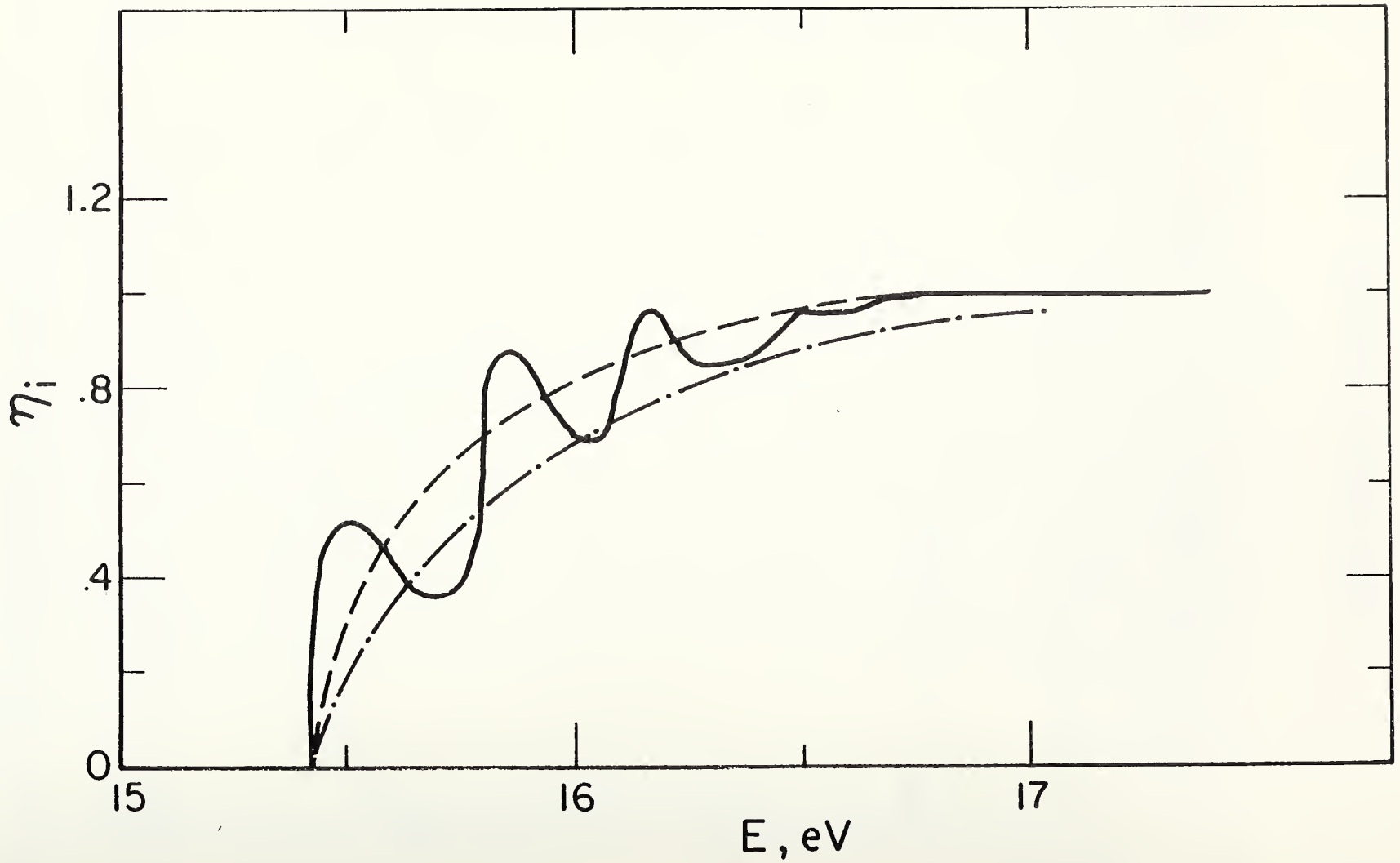

Fig. I.1 The ionization efficiency function as reproduced from [3]. The solid curve is due to Berkowitz [61]. The dashed line is a smoothed form due to Gerhart. The dash-dot line is due to eq (I.3).

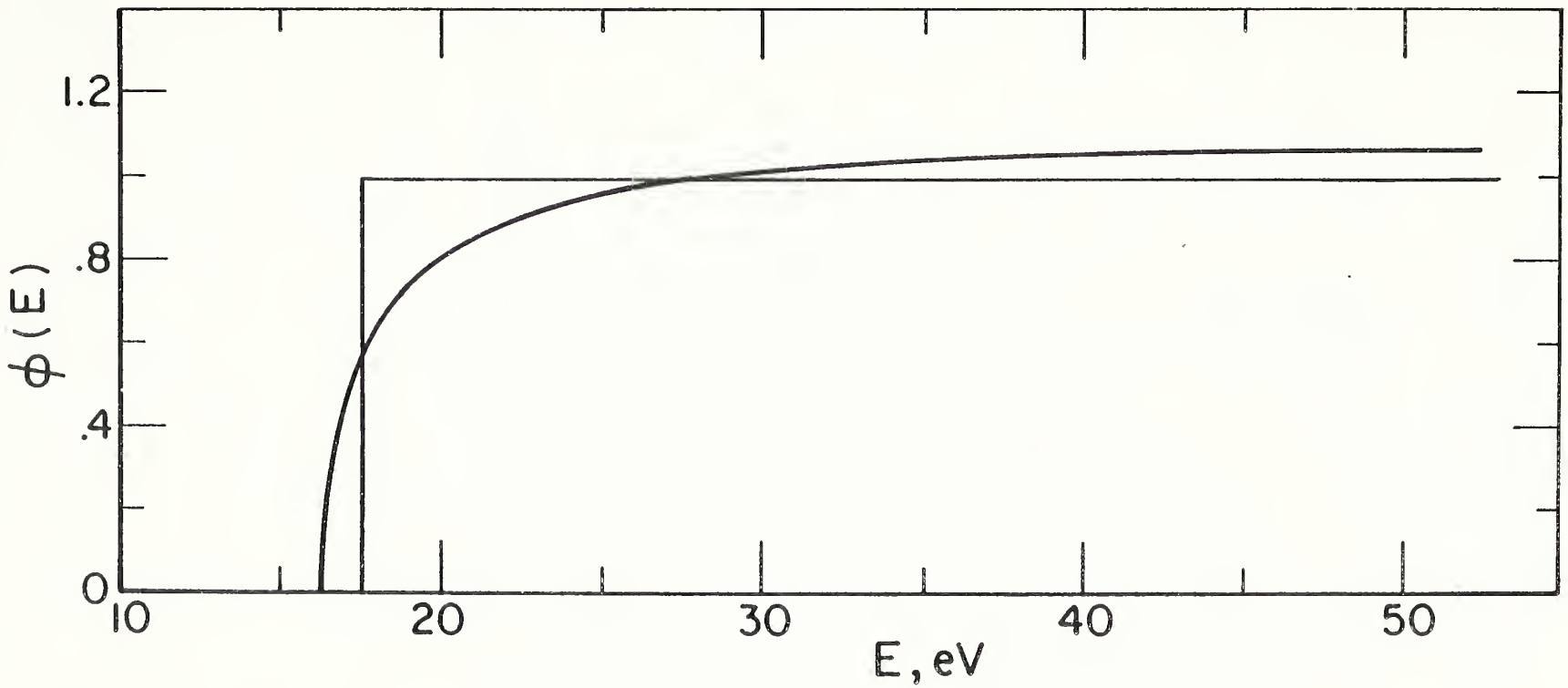

Fig. I.2 Gerhart's $\Phi(E)$ (heavy curve) is reproduced from his Fig. 6 [3]. The light curve expresses a unit function with cut-off at 17.5 eV.

REFERENCES

[1] D. A. Douthat, Electron energy degradation in molecular hydrogen. Radiological and Environmental Research Division Annual Report, ANL-76-88 170-176 (1976) Argonne National Laboratory, Argonne, Illinois. See also [54].

[2] R. H. Garvey, H. S. Porter, and A. E. S. Green, Relativistic yield spectra for H_2. J. Appl. Phys. 48, 4353-4359 (1977). See also A. E. S. Green, C. H. Jackman, and R. H. Garvey, Electron Inpact on Atmospheric Gases. J. Geophys. Res. 82, 5104-5111 (Nov. 1, 1977).

[3] Donald E. Gerhart, Comprehensive optical and collision data for radiation action. I. H_2. J. Chem. Phys. 62, 821-832 (1975).

[4] H. W. Lewis, Straggling effects on resonant yields. Phys. Rev. 125, 937-940 (1962).

[5] L. V. Spencer and U. Fano, Energy spectrum resulting from electron slowing down. Phys. Rev. 93, 1172-1181 (1954).

[6] Rosemary T. McGinnies, Energy spectrum resulting from electron slowing down. Nat. Bur. Stand., Circ. 597, 16 p. (1959).

[7] Daryl A. Douthat, Electron degradation spectra in Helium. Radiat. Res. 61, 1-20 (1975).

[8] U. Fano and L. V. Spencer, Quasi-scaling of electron degradation spectra. Int. J. Radiat. Phys. Chem. 7, 63-76 (1975).

[9] S. C. Soong, Inner-shell contributions to electron degradation spectra. Radiat. Res. 67, 187-214 (1976).

[10] D. A. Douthat, Energy deposition by electrons and degradation spectra. Radiat. Res. 64, 141-152 (1975).

[11] N. Bohr, On the decrease of velocity of swiftly moving electrified particles in passing through matter. Philos. Mag. and J. Sci. 30, 581-612 (1915).

[12] L. V. Spencer, and F. H. Attix, A theory of cavity ionization. Radiat. Res. 3, 239-254 (1955).

[13] P. R. J. Burch, Cavity ion chamber theory. Radiat. Res. 3, 361-378 (1955).

[14] Shin Sato, Kiyoshi Okazaki, and Shin-ichi Ohno, The estimation of the G-values for the ionization and excitation of noble gases irradiated by 100 keV electrons. Bull. Chem. Soc. Jap. 47, 2174-2180 (1974).

[15] Kiyoshi Okazaki and Shin Sato, Non-empirical calculation of the G-values for the ionization and excitations in diatomic molecules irradiated by 100 keV electrons. Bull. Chem. Soc. Jap. 48, 3523-3528 (1975).

[16] Cornelius E. Klots and Harvel Wright, Aspects of degradation spectra. Int. J. of Rad. Phys. and Chem. 2, 191-200 (1970).

[17] Martin J. Berger, Monte Carlo calculation of the penetration and diffusion of fast charged particles. Methods in Computational Physics, 1, Academic Press, Inc., NY, 135-215 (1963).

[18] D. O. Schneider and D. V. Cormack, Monte Carlo calculations of electron energy loss. Radiat. Res. 11, 418-429 (1959).

[19] Martin J. Berger, Spectra from energy degradation of fast electrons in water. Nat. Bur. Stand. Interim Report NBSIR 77-1283, 16 pages (1977).

[20] M. Jura, Ph.D. thesis (Harvard University, 1971), unpublished.

[21] A. Dalgarno and G. Lejeune, The absorption of electrons in atomic oxygen. Planet. Space Sci. 19, 1653-1667 (1971).

[22] T. E. Cravens, G. A. Victor, and A. Dalgarno, The absorption of energetic electrons by molecular hydrogen gas. Plant. Space Sci. 23, 1059-1070 (1975).

[23] Lennart R. Peterson, Discrete deposition of energy by electrons in gases. Phys. Rev. 187, 105-111 (1969).

[24] R. H. Garvey and A.E.S. Green, Energy-apportionment techniques based upon detailed atomic cross sections. Phys. Rev. 14A, 946-953 (1976).

[25] R. H. Fowler, Contributions to the theory of the motion of α-particles through matter. Part II, Ionizations. Proc. Cambridge Philos. Society 21, 531-541 (1923).

[26] L. R. Peterson and A.E.S. Green, The relation between ionization yields, cross sections and loss functions. J. Phys. B (Proc. Phys. Soc.) 1, Ser. 2, 1131-1140 (1968).

[27] Mitio Inokuti, D. A. Douthat, and A.R.P. Rau, Degradation spectra and ionization yields of electrons in gases. Proc. 5th Symp. Microdosimetry, Pallange, 977-1006 (22-26 September 1975).

[28] A.R.P. Rau, Ionization yields in gases on irradiation with charged particles: A variational approach. Annual Contract Report to NSF, Louisiana State University, Baton Rouge, LA, 23 pages (1976).

[29] Takeshi Namioka, Absorption spectra of H_2 in the vacuum-ultraviolet region. III. Potential-energy curves for the $B^1\Sigma_u^+$, $C^1\Pi_u$, $B'\ ^1\Sigma_u^+$, and $D^1\Pi_u$ states. J. Chem. Phys. 43, 1636-1644 (1965).

[30] C. B. Opal, E. C. Beaty, and W. K. Peterson, Tables of secondary-electron-production cross sections. Atomic Data 4, 209-253 (1972).

[31] R. D. DuBois and M. E. Rudd, Absolute doubly differential cross sections for ejection of secondary electrons from gases by electron impact. II. 100-500-eV electrons on neon, argon, molecular hydrogen, and molecular nitrogen. Phys. Rev. 17A, 843-848 (1978).

[32] A.E.S. Green, Jan. 23, 1978 letter, unpublished.

[33] Donald Rapp and Paula Englander-Golden, Total cross sections for ionization and attachment in gases by electron impact. I. Positive ionization. J. Chem. Phys. 43, 1464-1479 (1965).

[34] Martin J. Berger, Spectra from energy degradation of fast electrons in water. NBSIR 77-1283, 15 pages (August 1977), NBS Interagency Report (unpublished).
M. J. Berger and S. M. Seltzer, Calculation of energy and charge deposition and of the electron flux in a water medium bombarded with 20-MeV electrons. Annals of the New York Academy of Sciences, 161, 8-23 (1969).

[35] William P. Jesse and John Sadaukis, Absolute energy to produce an ion pair by beta particles from S^{35}. Phys. Rev. 107, 766-771 (1957).
Ionization in pure gases and the average energy to make an ion pair for alpha and beta particles. Phys. Rev. 97, 1668-1670 (1955).

[36] G. G. Meisels, Gas-phase dosimetry by use of ionization measurements. J. Chem. Phys. 41, 51-56 (1964).

[37] Jerome Weiss and William Bernstein, Energy required to produce one ion pair in several noble gases. Phys. Rev. 103, 1253 (1956).

[38] Roger M. Leblanc and Jan A. Herman, Determination des valeurs W_β pour les gaz et vapeurs organiques par la methode des courants de saturation. J. Chim. Phys. 63, 1055-1060 (1966).

[39] J. F. Lehmann, The absorption of slow cathode rays in various gases. Proc. Roy. Soc. A115, 624-639 (1927).

[40] W. C. Barber, Specific ionization by high-energy electrons. Phys. Rev. 97, 1071-1077 (1955).

[41] J. M. Valentine, Energy per ion pair for electrons in gases and gas mixtures. Proc. Royal Society of London, Series A. Mathematical and Physical Sciences 211, 75-85 (Cambridge University Press, Bentley House, N.W. 1 March, 1952).

[42] Leon M. Dorfman, Absorption of tritium beta particles in hydrogen and other gases. Phys. Rev. 95, 393-396 (1954).

[43] William P. Jesse and John Sadauskis, Alpha-particle ionization in pure gases and the average energy to make an ion pair. Phys. Rev. 1120-1121 (1953).

[44] T. E. Bortner and G. S. Hurst, Ionization of pure gases and mixtures of gases by 5-MeV alpha particles. Phys. Rev. 93, 1236-1241 (1954).

[45] C. Biber, P. Huber, and A. Müller, Arbeit pro Ionenpaar von mehratomigen gasen für Po-α-Teilchen. Helvetica Physica Acta 28, 503-521 (1955).

[46] C. J. Bakker and E. Segrè, Stopping power and energy loss for ion pair production for 340-MeV protons. Phys. Rev. 81, 489-492 (1951).

[47] Cornelius E. Klots, Energy-partition parameters in radiation studies of molecular gases. J. Chem. Phys. 44, 2715-2718 (1966).

[48] Georg Stetter, Die ionisation einzelner alpha-strahlen in verschiedenen gasen. Z. Physik (H. Geiger, ed.) 120, 639-651 (1943).

[49] W. Riezler and A. Rudloff, Ionisation und Energieverlust von alpha-teilchen in verschiedenen gasen. Annalen der Physik. 15, 224-245 (1955).

[50] J. M. Valentine and S. C. Curran, Energy Expenditure per ion pair for electrons and α-particles. Philosophical Magazine 43, 7th Series, 964-967 (Prof. N. F. Mott, ed., 1952).

[51] W. M. Jones, Some calculated quantities in the radiation chemistry of molecular hydrogen: Average energy per ion pair and numbers of singlet and triplet excitations per ion pair. J. Chem. Phys. 59, 5688-5695 (1973).

[52] G. D. Alkhazov, Ionization fluctuations in gases. Soviet Physics-Technical Physics 16, 1540-1545 (1972).

[53] A. Dalgarno and G. W. Griffing, Energy per ion pair for electron and proton beams in atomic hydrogen. Proc. Roy. Soc. A248, 415-428 (1958).

[54] D. A. Douthat, Energy deposition and electron energy degradation in molecular hydrogen. Submitted to J. Phys. B.

[55] R. L. Platzman, Total ionization in gases by high-energy particles: An appraisal of our understanding. Int. J. Appl. Radiation and Isotopes, 10, 116-127 (1961).

[56] G. N. Whyte, Energy per ion pair for charged particles in gases. Radiat. Res. 18, 265-271 (1963).

[57] D. Combecher, private communication to M. Inokuti (Feb. 20, 1978).

[58] William Frederick Miller, A theoretical study of excitation and ionization by electrons in helium and of the mean energy per ion pair. Ph.D. Thesis, Purdue U., 166 pages (1956).

[59] A. C. Allison and A. Dalgarno, Band oscillator strengths and transition probabilities for the Lyman and Werner systems of H_2, HD, and D_2. Atomic Data 1, 289-304 (1970).

[60] G. R. Cook and P. H. Metzger, Photoionization and absorption cross sections of H_2 and D_2 in the vacuum ultraviolet region. J. Opt. Soc. Am. 54, 968-972 (1964).

[61] J. Berkowitz, unpublished.
J. Berkowitz and W. A. Chupka, Photoelectron spectroscopy of autoionization peaks. J. Chem. Phys. 51, 2341-2354 (1969).
W. A. Chupka and J. Berkowitz, High-resolution photoionization study of the H_2 molecule near threshold. J. Chem. Phys. 51, 4244-4268 (1969).

[62] Mitio Inokuti, Inelastic collisions of fast charged particles with atoms and molecules--The Bethe Theory revisited. Rev. Mod. Phys. 43, 297-347 (1971).

[63] H. Ehrhardt, L. Langhans, F. Linder, and H. S. Taylor, Resonance scattering of slow electrons from H_2 and CO angular distributions. Phys. Rev., 173, 222-230 (1968).

[64] S. Trajmar, D. G. Truhlar, J. K. Rice, and A. Kuppermann, Electron scattering by H_2 with and without vibrational excitation. III. Experimental and theoretical study of inelastic scattering. J. Chem. Phys. 52, 4516-4533 (1970).

[65] H. Bethe, Quantenmechanik der Ein- and zwei-electronenprobleme. Handbuch der Physik, 24, Kapitel 3 (H. Geiger and Karl Scheel, Eds.) München, Germany, 18-560 (see p. 519 ff) (1933).

[66] M. Bogaardt et B. Koudijs, Sur les potentiels moyens d'excitation et les relations énergie-parcours dans les éléments légers. Physica 18, 249-264 (1952).
G. Mano, Recherches sur l'absorption des rayons, Annales de Physique, Series 11, 1, 407-531 (1934).

[67] F. W. Martin and L. C. Northcliffe, Energy loss and effective charge of He, C, and Ar ions below 10 MeV/amu in gases. Phys. Rev. 128, 1166-1174 (1962).

[68] U. Fano, Penetration of protons, alpha particles, and messons. Annual Reviews of Nuclear Science 13, 1-66 (1963).

[69] Joseph F. Janni, Calculations of energy loss, range, pathlength, straggling, multiple scattering, and the probability of inelastic nuclear collisions for 0.1- to 1000-MeV protons. Air Force Weapons Laboratory, Technical Report No. AFWL-TR-65-150, Kirtland Air Force Base, New Mexico, 438 pages (Sept. 1966).

[70] P. H. Garbincius and L. G. Hyman, Range-energy relation in hydrogen. Phys. Rev. 2A, 1834-1838 (1970).

[71] Lucien Pages, Evelyne Bertel, Jemro Joffre, and Laodamas Sklavenitis, Energy loss, range, and bremsstrahlung yield for 10-keV to 100-MeV electrons in various elements and chemical compounds. Atomic Data 4, 1-127 (1972).

[72] T. J. Thompson, Effect of chemical structure on stopping powers of high-energy protons, Univ. Calif. Radiation Laboratory Report UCRL-1910, Univ. Calif. Radiat. Lab. Berkeley, pages (1952).

[73] G. D. Zeiss, William J. Meath, J.C.F. MacDonald, and D. J. Dawson, Accurate evaluation of stopping and straggling mean excitation energies for N, O, H_2, N_2, O_2, NO, NH_3, H_2O, and N_2O using dipole oscillator strength distributions. Radiat. Res. 70, 284-303 (1977).

[74] J. D. Garcia, Radiative corrections to the energies of atoms and molecules. Phys. Rev. 147, 66-68 (1966).

[75] G. A. Victor and A. Dalgarno, Dipole properties of molecular hydrogen. J. Chem. Phys. 50, 2535-2539 (1969).

[76] P. W. Langhoff and A. C. Yates, Moment theory bounds on the mean energies of stopping, straggling, and molecular excitation. J. Phys. B: Atom. Molec. Phys. 5, 1071-1081 (1972).

[77] A. Lewis Ford and J. C. Browne, Direct-resolvent-operator computations on the hydrogen-molecule dynamic polarizability, Rayleigh, and Raman scattering. Phys. Rev. 7A, 418-426 (1973).

[78] G. D. Zeiss, William J. Meath, J.C.F. MacDonald, and D. J. Dawson, Dipole oscillator strength distributions, sums, and some related properties for Li, N, O, H_2, N_2, O_2, NH_3, H_2O, NO, and N_2O. Can. J. Phys. 55, 2080-2100 (1977).

[79] J. E. Turner, Patricia D. Roecklein, and R. B. Vora, Mean excitation energies for chemical elements. Health Phys. 18, 159-160 (1970).

[80] H. H. Andersen and J. F. Ziegler, The Stopping and Ranges of Ions in Matter, 3, Hydrogen stopping powers and ranges in all elements, 317 pages (1977).

[81] Werner Brandt, Survey of stopping power. Health Phys. 1, 11-20 (1958).

[82] Hans Bichsel, Passage of charged particles through matter. American Institute of Physics Handbook, 3rd Edition, 8, 142-189 (1972).

[83] Jochen Booz and Heinrich Georg Ebert, Mittlerer Energieaufwand W zur Bildung eines Ionenpaares in Gasen durch Electronen, Beta-, Gamma- und Röntgenstrahlung. Strahlentherapic 120, 7-33 (1963).

[84] E. J. Williams, Correlation of certain collision problems with radiation theory, Vid. Selsk. Math.-fys. Medd. XIII, 4, 50 pages (1935).

NBS-114A (REV. 7-73)

U.S. DEPT. OF COMM. BIBLIOGRAPHIC DATA SHEET	1. PUBLICATION OR REPORT NO.	2. Gov't Accession No.	3. Recipient's Accession No.

4. TITLE AND SUBTITLE

Numerical Solution of the Electron Slowing-Down Equation for Molecular Hydrogen

5. Publication Date

6. Performing Organization Code

7. AUTHOR(S)

I. V. Spencer and R. Pal

8. Performing Organ. Report No.

9. PERFORMING ORGANIZATION NAME AND ADDRESS

NATIONAL BUREAU OF STANDARDS
DEPARTMENT OF COMMERCE
WASHINGTON, D.C. 20234

10. Project/Task/Work Unit No.

5331439

11. Contract/Grant No.

12. Sponsoring Organization Name and Complete Address *(Street, City, State, ZIP)*

13. Type of Report & Period Covered

14. Sponsoring Agency Code

15. SUPPLEMENTARY NOTES

16. ABSTRACT *(A 200-word or less factual summary of most significant information. If document includes a significant bibliography or literature survey, mention it here.)*

Procedures are outlined for solution of the slowing-down equation for fast electrons in differential form rather than in one of its integral forms. Data for H_2 are computed by use of Gerhart's cross section set, suitably modified, and with inclusion of vibrations. The flexibility and stability of the approach is demonstrated by solutions for source energies ranging from 1 MeV down to 24 eV with the spectrum extended below 2 eV. Energy and number conservation are checked in detail, and the ionization yield is computed as a function of energy. Spectrum and ionization yield so obtained are compared with previous calculations; general agreement is found with some significant differences. Agreement with Combecher's measured ionization yields at low energies is rather satisfactory overall, but with significant deviations of trend. Some exploration of secondary and tertiary electron contributions is included.

17. KEY WORDS *(six to twelve entries; alphabetical order; capitalize only the first letter of the first key word unless a proper name; separated by semicolons)*

Electron slowing-down; energy degradation spectrum; inelastic cross section set; ionization yield; molecular hydrogen; W-value.

18. AVAILABILITY

☐ Unlimited

☒ For Official Distribution. Do Not Release to NTIS

☐ Order From Sup. of Doc., U.S. Government Printing Office Washington, D.C. 20402, SD Cat. No. C13

☐ Order From National Technical Information Service (NTIS) Springfield, Virginia 22151

19. SECURITY CLASS (THIS REPORT)

X
UNCLASSIFIED

21. NO. OF PAGES

100

20. SECURITY CLASS (THIS PAGE)

UNCLASSIFIED

22. Price